Gasification of N-rich fibreboard in an air-blown fluidized bed reactor: A study on the fate of tars, NH3 and HCN during oxidative mild Hot Gas Filtration

M. Ruiz, A. Schnitzer, P. Arnoux, G. Mauviel

Gasification of N-rich fibreboard in an air-blown fluidized bed reactor: A study on the fate of tars, NH_3 and HCN during oxidative mild Hot Gas Filtration.

Authors and affiliations:

M.Ruiz[a], A. Schnitzer[a,b], P. Arnoux[a], G.Mauviel[a]

[a]LRGP, CNRS, University of Lorraine, ENSIC, 1 Rue Grandville, Nancy, France

[b]University of Lorraine, LERMaB, ENSTIB, 27 Rue Philippe Séguin, PO Box 1041, F-88051 Epinal, France

Corresponding author:

Miguel Ruiz (Miguel.ruiz@keemail.me)

1. Introduction

Gasification is a thermochemical conversion route to transform biomass and wastes to a gas vector (syngas) with proven potential to replace fossil fuels in the production of heat, power and chemicals. When air is employed as gasification agent, the resulting syngas is diluted by N_2 and, generally referred as producer gas. Producer gas typically presents pollutants, such as: char/ash particles, tars and inorganic gases that restrain its applications and jeopardize long term operation of gasification plants. To resolve this issue, several physical, chemical and catalytic clean-up strategies have been developed [1–3]. Depending on their positioning in the gasification system they can be classified as primary and secondary methods. The combination of primary and secondary methods has shown high efficiency in the reduction of pollutants but, as a general rule-of-thumb, the overall economy of the process will be negatively affected with increasing complexity of the clean-up system. Ergo, developing simple and inexpensive producer gas clean-up strategies is necessary to foster the development of the gasification route.

Hot Gas Filtration (HGF) is a robust and simple clean-up technique with proven efficiency to simultaneously remove dust particles and reduce tar concentration [4]. When a HGF is coupled downstream a gasification reactor, particles transported in the producer gas flow are retained on the filter surface and form the filter cake. These particles, hereafter referred as “dust”, include char, soot, ash and material elutriated from the reactor in the case of fluidized bed reactors. The filter cake build-up presents two major outcomes. Firstly, dust particles, in particular char, can act as heterogeneous catalyst for tar abatement. Secondly, as the dust cake builds-up, the pressure drop across the filter increases continuously compromising the long-term operation of the system. Because of their high importance these two key aspects are discussed hereafter.

Catalytic activity of char for the abatement of tar is known and already exploited in the operation of staged gasification reactors [5]. In contrast to metal and mineral catalysts, chars are by-products of the gasification process and thus, cost-free materials. These two advantages explain the increasing interest of the community to unveil the reactional pathways and kinetics of tar decomposition reactions when char is used as catalyst. Available literature about the decomposition of tar model compounds over activated/non-activated char has been recently reviewed [6,7]. Main conclusions from these studies are summarised below:

- Catalytic activity of char particles depends on several factors mainly related to the physicochemical properties and structure of the parent biomass particles, the char production parameters and the heterogeneous reaction conditions, in particular, the reaction temperature.
- Carbon deposition (or coking) is the main mechanism of the decomposition of model tar molecules.
- Coking leads to the loss the catalytic activity of char particles. Nevertheless, catalytic activity can be maintained if gasification rate of char/coke is equivalent or greater than the coke formation rate.

Although studies conducted under simulated environment are abundant and provide fundamentals, HGF studies performed on real producer gas environment at bench/pilot scale are scarce. Indeed, few data are available regarding the impact of dust particles accumulated on the HGF surface on the composition and yields of pollutants. Tuomi and co-workers [8] studied the behaviour of tars produced from steam and air/steam atmospheric bubbling-bed gasification reactor coupled with a HGF kept at 800°C and equipped with ceramic candles. GC-MS characterization of tars samples recovered upstream and downstream the HGF unit revealed a decrease in total tars concentration regardless of the used feedstock, bed material or gasifying agent but, contradictory results were found regarding the impact of HGF on the heaviest tar fraction. Moreover, Chun-Zhu Li and co-

68 workers [9–11] integrated a char fixed bed on the top of a pilot plant gasification reactor to perform
69 hot gas cleaning of producer gas using char and iron loaded biomass char and coal catalysts. UV-
70 fluorescence spectroscopy analysis of tar samples indicated that iron loaded char was the most
71 active catalyst in the decomposition of large aromatic ring compounds. Furthermore, catalyst
72 integration in HGF candles is a strategy with great potential to reduce tar in producer gas [12–16].
73 However, higher cost and limited lifespan of the catalytic elements currently jeopardize its
74 application into an industrial scale.

75 Long term operation is a key issue in HGF units. Two phenomena are closely linked to the progressive
76 loss in filter permeability. First, slag formation due to irreversible ash aggregation and sintering. This
77 phenomenon is generally intensified for filtration temperatures above 600°C and ash-rich feedstocks
78 [4], although stable filter operation can be achieved even at filtration temperatures close to 800°C
79 provided that bed material and back pulse parameters are carefully chosen [17]. Second, the
80 formation of a soot-rich sticky layer on the surface of the filter. This phenomenon is generated by the
81 polymerization of high molecular weight tar species and amplified in the case of a particle-poor and
82 tar-rich producer gas [18]. Oxidative HGF has been shown to provide a simple solution to overcome
83 this issue. Indeed, the oxidation of the soot-rich sticky layer is accomplished by the injection of an
84 additional air flow into the filter vessel. Lang et al.[19] performed oxidative filtration tests on an
85 air/steam blown 1 MW_{th} mixed-draft fixed-bed biomass gasifier at a filtration temperature between
86 400-600°C. These authors reported dust and tar removal efficiencies greater than 90% with stable
87 pressure drop for over 200 h but, no information was given regarding the impact of oxidative hot gas
88 filtration neither on the composition of tars nor on the content of acid gases.

89 In this study, the HGF strategy applied differs from the previous approach used for HGF in gasification
90 processes. First, in our system, no back-pulse system was used to remove the dust cake accumulated
91 on the filter surface during the HGF tests. The purpose of keeping in place the dust cake was to
92 promote heterogeneous reactions between the dust cake particles and the producer gas. Second, the

93 filtration temperature targeted inside the HGF unit was in a “mild” range between 400-600°C.
94 Although the temperature targeted might be low to promote tar conversion, which is known to
95 become significant above 800°C [20], this mild temperature range was selected to reduce the
96 formation of ash deposits on the filter surface and thus, limit the irreversible agglomeration, melting
97 and sintering of ash in the porosity of the filter. Additionally, regarding construction cost of the HGF
98 unit, the utilisation of mild filtration temperature reduces the material requirements and thus, their
99 cost. Third, in this study, a new technology of multilayer metallic filtration cartridges was selected
100 instead of ceramic candles. Fourth, and similarly to the research conducted by Lang and co-workers
101 [19], a controlled flow of secondary air was injected in the mainstream of producer gas at the entry
102 of the HGF unit.

103 Therefore, using this innovative strategy of oxidative HGF, a N-rich feedstock, consisting in pellets of
104 Medium Density Fibreboard (also known as MDF), was gasified in an air-blown bubbling bed reactor
105 at 800°C coupled with the downstream HGF unit. To the best of our knowledge, studies dealing with
106 the gasification of MDF feedstocks are scarce in literature and mostly concerns the thermal
107 degradation studies conducted under pyrolysis conditions [22,23]. Williams et al. [24] carried out
108 several gasification experiments with briquetted MDF feedstock in a down-draft air-blown reactor
109 coupled with a diesel engine generator. Authors reported smooth operation of the system and
110 calorific values of producer gas identical to those of standard hardwood chip fuels but, yet again, no
111 information was communicated on pollutant content of the gas. The present study seeks to address
112 this gap by the utilisation of complementary analytical techniques to map the fate of tars and
113 nitrogen derived species (NH_3 and HCN) during oxidative HGF. The effects of the secondary air flow
114 rate and the dust loading on gasification indicators and pollutant content were also investigated.
115 Additionally, filter clogging mechanisms were investigated based on SEM-EDX analyses of the filter
116 surface.

2. Materials and methods

2.1. Feedstock material

Feedstock material used in this study was Medium Density Fibreboard (MDF) waste from the furniture industry provided by RAGT Energy (Albi, France). Grinding of waste MDF produced a very low-density fluffy material with poor bulk flowability that systematically blocked the screw feeding system of the gasifier. To avoid flowability issues, the MDF fluffy material was pelletized. Table 1 presents proximate, ultimate analysis and elemental ash composition of the feedstock material. Proximate analysis was conducted according to French standards NF EN ISO18134. Ultimate analysis was conducted according to standards ISO 16948 and ISO 16994. MDF typically presents a high content in Fuel Bounded Nitrogen (FBN) due to the utilisation of urea-formaldehyde resin for its production. Ash melting temperatures of biomass samples were determined according to French standard CEN/TS 15370-1.

Table 1: Feedstock analyses.

Composition of MDF feedstock	
Moisture, wt.%	8.6
Volatile content, wt.% (db)	88
Ash wt. % (dry base)	0.42
Ultimate analysis, wt.%(db)	
C	49.6
H	6.02
N	3.47
S	0.008
Cl	0.005
$O_{calculated\ by\ difference}$	40.48
Major metallic elements in Ash composition, mg/kg$_{feedstock}$ (db)	
Ca	791
K	890
Mn	111
Mg	274
Na	61
P	91
Si	<100
Minor metallic elements in Ash composition, mg/kg$_{feestock}$ (db)	
As	<0.8
Al	45
Cd	<0.2
Cr	<1
Cu	1
Fe	41

Ni	<1
Pb	<2
Zn	16
Hg	<0.05
Co	<1
Mo	<2
Ti	3
Sb	<1
V	<1
Ash melting temperatures (°C)	
Initial deformation temperature	1070
Softening temperature	1420
Hemispherical temperature	1460
Fluid temperature	1490

130

131 2.2. Pilot-scale fluid bed gasification reactor system

132 A scheme of the pilot-scale gasification rig is depicted in Figure 1. Main elements of the experimental
133 rig are fully described elsewhere [25]. For the present study, several modifications have been carried
134 out with respect to the original system, in particular, regarding the fuel feeding system and feed
135 injection point, as well as, the pollutant sampling set-up.

136

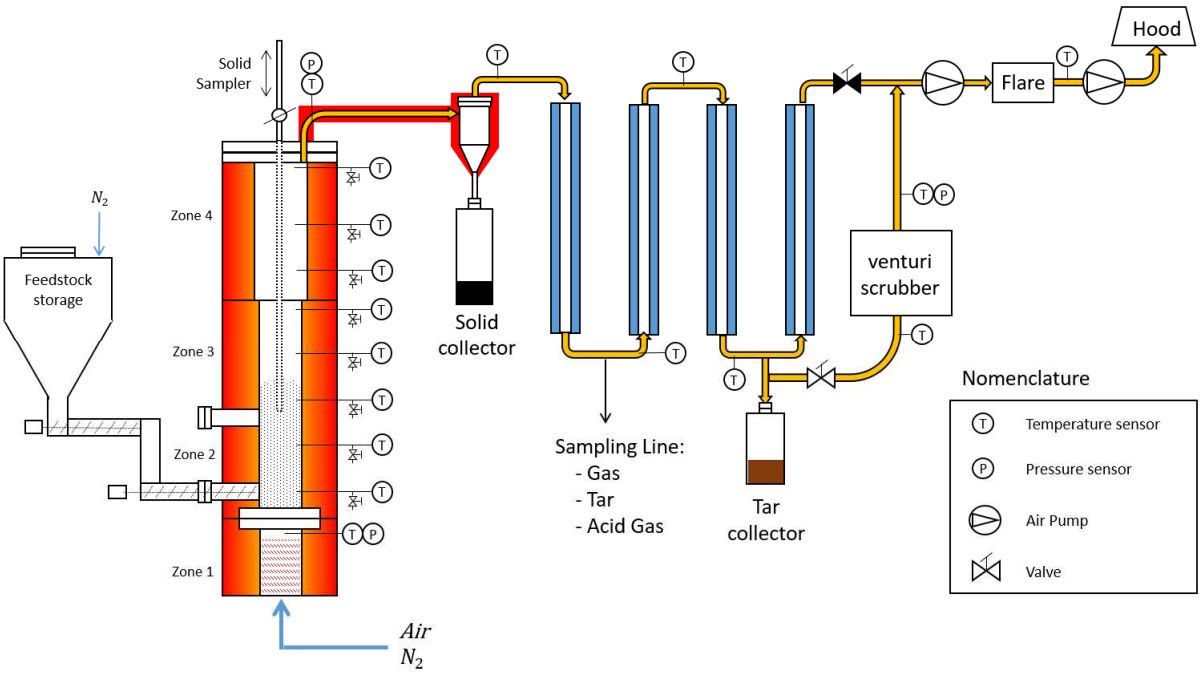

137

138 **Figure 1: Scheme of the pilot-scale gasification rig. A picture of the installation was included in Appendix A.**

Briefly, the experimental rig was composed of 4 main modules: (i) a continuous fuel feeding system, (ii) a bubbling fluidized bed reactor, (iii) a cyclone and, (iv) a gas cooling and wet scrubbing cleaning system. Feedstock material was continuously introduced from the fuel tank to the reactor bed, approximately 15 mm above the distributor plate, by a double screw system. 20 L/min (STP) of pure nitrogen was continuously feed through the feedstock alimentation system for inertization and pressure stabilisation purposes. The gasification reactor was divided into three zones: the plenum (d=100mm, H=300mm), the bed zone (d=100mm, H=800mm), and the freeboard zone (d=140mm, H=800 mm). The reactor was externally heated by four electrical resistances and thermally insulated. Air was used as gasifying agent in all experiments. Primary air was injected at constant flow 4540 NL/h (Brooks 5851s) into the plenum zone of the reactor. Additionally, a second flowmeter (Brooks 5850s) was installed in parallel to assure system purge operations with pure nitrogen if required. For each test, 4 kg of fresh olivine (VANGUARD™, SIBELCO) was used as bed material (particle size 200-600 µm). Fluidisation velocity was two times greater than the minimal fluidisation velocity (U_{mf}) equals to 0.3 m/s at 800°C (as measured in this set-up). Under these conditions, gas residence time inside the reactor was 4 s. Downstream of the gasification reactor, coarse solid particles were removed from the main gas stream with a cyclone separator. Then, the producer gas was cooled down in three heat exchangers before introduction in a wet venturi scrubber. To compensate pressure-drop across the gasification rig, a side channel blower (SCL 06R, EFFEPIZATA) was installed downstream the venturi scrubber and operated at constant flow rate during the tests. Finally, the producer gas was burned before evacuation.

To carry out the filtration experiments, the cyclone separator was replaced by a HGF unit. A scheme of the HGF unit is depicted in Figure 2. The HGF unit was composed of a preheating zone, a gas mixing zone and a filter housing; each zone was electrically heated and thermally insulated. For all HGF tests, the temperature set-point of the filter housing heating system was fixed at 450°C. The temperature inside the HGF unit was continuously measured at different points (see Figure 2). Multilayer filtration cartridges, provided by the company GKD (Düren, Germany) [21], consisted of an

outer thin metal fabric with a mean pore size of 10 µm followed by a 2-3 mm layer of non-woven metal fibres supported on a metallic frame. To the best of our knowledge, these filters were used for the first time downstream a gasifier. Two sets of two metallic cartridges each (ID=40 mm, ED= 60mm, L=600 mm) were used in this study. No back-pulse system was employed in any of the filtration tests in order to increase the contact time between the filter cake and the producer gas. Filter cake oxidation was accomplished by the injection of a secondary air flow into the HGF unit. The temperature of the secondary air flow could be independently modulated by a preheater but, for all filtration experiments, the preheater was switched off and the secondary air flow was injected at ambient temperature. The main operational parameters of the HGF unit are detailed in Table 2. Face filtration velocity was calculated as the ratio between the flowrate of producer gas and the total filtration surface (see Equation A.1, Appendix A).

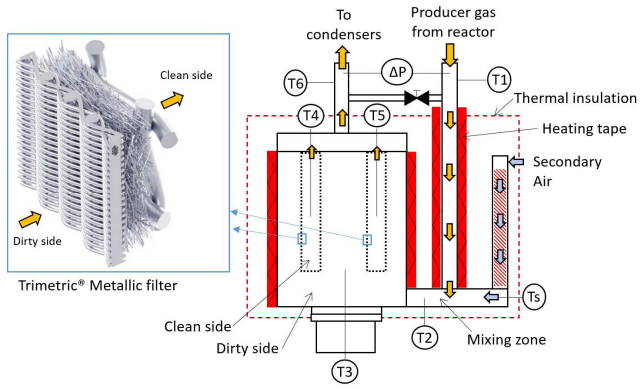

Figure 2: A schematic view of the hot gas filtration unit and the multilayer metallic filter mesh. Thermocouple T2 measured the temperature of the mixing zone and T3 measured the temperature of the dirty side. The temperature of the clean gas side was calculated as the average temperature measured by thermocouples T4 and T5, placed at the clean side of the filtration cartridges.

2.3. Sampling and Analytical methods

Permanent gases, tars and acid gases contained in the producer gas were sampled downstream of the first heat exchanger where the temperature of the producer gas was between 350 and 400 °C. A small flow of producer gas (5 to 7 L/min, STP) was continuously derived from the mainstream and

sent through a heated line kept at 450°C to three sampling trains, namely: the µGC, the tar protocol and the acid gas. Figure 3 depicts a scheme of the sampling system.

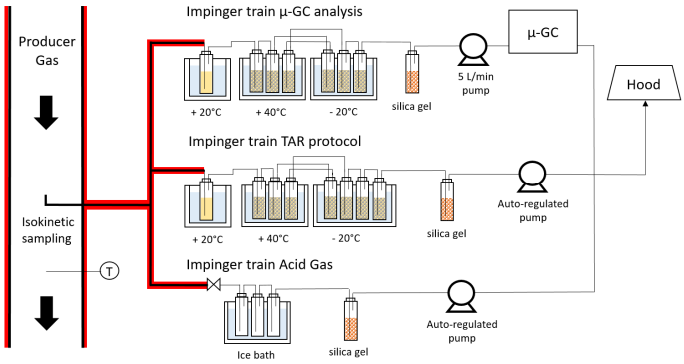

Figure 3: Scheme of the sampling system.

Producer gas composition was measured by a µGC analyser (Variant micro-GC 490, 4 modules) every 3 minutes. To avoid line clogging, producer gas was continuously scrubbed through an impinger train composed of 7 impinger bottles filled with glass beads (OD 5 mm) and 2-propanol. A bottle filled with silica gel balls was placed downstream the impinger train to adsorb moisture and protect the pump. N_2, CO, CO_2, H_2, CH_4, C_2H_2, C_2H_6, C_3H_4 and C_3H_6 were quantified by this technique using N_2 as a tracer.

Tar quenching was carried out based on a version of the standard method described in the European Tar Protocol (CEN/TS 15439). A volume of 60 L (STP) of gas was scrubbed at 2 L/min through an impinger train composed of 8 impinger bottles (500 mL) with 2-propanol (analytic grade). To assure stable pressure drop across the impinger line, frits were replaced by glass balls beads (OD 5 mm). The volume of the glass balls beads was about 400 ml. The configuration of the impinger train is detailed in Table A.1 (Appendix A). Liquid from the impingers 1 to 7 was added in a recipient and stocked at 15°C until analysis. Collection efficiency of the impinger train was systematically verified by analysing separately the liquid collected in impinger n°8 by HPLC and GC/MS-FID. A bottle filled with silica gel balls was placed downstream the impinger train to protect the pump. The precise volume of sampled gas was measured with an auto-regulated pump (Gilian GilAir Plus) and corrected to standard

pressure and temperature. Impinger bottles and glass beads were thoroughly washed with acetone after utilisation. Compared to other tar sampling methods, such as Solid Phase Adsorption [26], relatively long sampling time (approx. 30 min) used in the wet method reduced the uncertainty linked to the fluctuations on the composition and tar content of producer gas along the time, as a result of small variations in the feed throughput. However, longer sampling time and labour required for the wet sampling method prevent its utilisation for time resolved tar analysis.

Low molecular weight tar species were quantified with a simplified version of the GC*GC/MS-FID-FID method fully described elsewhere [27]. Briefly, one microliter of the solution (sample and internal standard) recovered from tar protocol was injected with a split ratio 1:50 in an Agilent 7890 gas chromatographer (HP-5MS column). The oven temperature program was: 50°C hold (hold for 7 min), then increased at 10 K/min to 250°C (hold for 20 min). The exit of the HP-5MS was connected simultaneously to the FID and to the MS detectors. Quantification was carried out according to predictive FID response factor method of de Saint Laumer [28], using 1-tetradecene as internal standard. A list of low Mw molecules quantified by this method can be found in Table A.2 (Appendix A).

Quantitative analysis of high molecular tar species (Polycyclic aromatic hydrocarbons or PAH) was conducted by HPLC (Shimadzu SCL-10Avp) coupled to UV detection (Shimadzu SPD 10Avp) operated at 254 nm. Standard calibration lines were calculated for five levels of standard concentration (TCL 16 PAH Mix, Supelco) and each point was repeated at least 2 times. A PHENOMENEX Envirosep PP C18 column (5 µm particle size, 125 mm x 4.6 mm i.d.) was operated at ambient temperature with a Shimadzu LC 10 ADvp pump. An elution gradient was applied using acetonitrile/water at a flow rate of 0.8 ml/min. The injection volume was 10 µl. A list of high Mw molecules quantified by this method can be found in Table A.2 (Appendix A).

Semi-Quantitative analysis of overall tar composition was conducted by UV-Absorbance (UV-A) and Synchronous Fluorescence Spectroscopy (SFS). Absorption spectra were recorded on a Shimadzu UV-

3600 UV-visible double beam spectrophotometer using a standard quartz cell with 1 cm path length and 2-propanol as blank. Emission and Synchronous Fluorescence (SF) spectra were recorded on a Horiba spectrofluorimeter Fluorolog FL3-222 equipped with 450 W Xenon lamp, a thermo-stated cell compartment (25°C) and a Hamamatsu UV-visible photomultiplier R928. To perform semi-quantitative analysis, all analytical solutions were prepared by dilution in 2-propanol to 5000 ppm (v/v). Analytical concentration was previously determined to obtain an absorbance value of 0,25 at a wavelength value of 254 nm for a sample corresponding to the reference tests. Indeed, a high dilution ratio of analytical samples is known to minimise the quenching effect while ensuring a high dependence between the structure of a given PAH family and the spectral profile [29]. Moreover, the SF spectra were recorded in a range between 200 and 600 nm with an offset ($\Delta\lambda$) of 3 and 20 nm and a bandwidth of 2 nm. The values of $\Delta\lambda$ used in this study were selected with different analytical purposes. On the one hand, the SF spectra recorded at $\Delta\lambda$=3 nm gives a precise fingerprint of the sample composition due to the reduction of spectral bandwidth and thus, of spectral overlaps [30]. On the other hand, the SF spectra recorded at $\Delta\lambda$=20 nm represent an acceptable trade-off between the spectra intensity for most of PAH molecules and the spectra resolution, providing an overall vision of the "gross" composition of the sample [31]. Furthermore, considering the heterogeneity of $\Delta\lambda$ values and solvents employed in literature for the acquisition of the SF spectral data of aromatics and model PAHs molecules, the SF spectra these molecules, typically present in high concentration in the reference tests tar samples, were determined. Finally, to take into account the "dilution effect" of the SF spectra (as a result of the injection of secondary air in the HGF unit), fluorescence intensity was normalised with the volume of gas sampled and then, multiplied by the gas yield defined by Equation B.2 (Appendix B).

Inorganic gases NH_3 and HCN were quenched separately in two impinger trains consisting in three glass impingers with frit, placed in series and kept in an ice bath (Figure 3). A bottle filled with silica gel balls was placed downstream the impinger train to protect the pump. The sampling procedure was adapted from previous articles [32,33]. Briefly, 150 mL of acid (H_2SO_4 0.1N) and basic (NaOH

0.1M) solution was poured in each impinger and cooled for 20 min in the ice bath before quenching. A volume of 5 L (STP) of gas was sampled at 1 L/min with an auto-regulated pump (GilAirPlus, GILIAN) and corrected to standard pressure and temperature. Liquid recovered in each impinger was analysed separately to verify the collection efficiency. All samples were stored at -7°C until analysis. Quantification of targeted ions was carried out by ion chromatography according to French standards: NF X43 303 for NH_3 and NF T90-107 for HCN.

Filter dust cake particles were dislodged from the filter cartridge by gentle shaking and thoroughly mixed to assure homogeneity prior to analysis. Analytical techniques used for the characterisation of cyclone and dust cake particles include: elemental analysis, carried out with a Thermo Fisher apparatus (Flash EA 1112), and inorganic element quantification by ICP-AES, carried out according to French standards NF EN ISO 16967 and NF EN ISO 16968. Additionally, the PAH content of solid particles recovered from the cyclone and the filter dust cake was compared by Synchronous Fluorescence Spectroscopy after solvent extraction. Briefly, both samples were extracted with 2-propanol (0.1 g of solid / 100 mL of solvent) for 3 days under agitation at 30°C. Solutions were filtered (0.45 µm) and then analysed by SFS at $\Delta\lambda$=20 nm without dilution. Finally, a Scanning Electron Microscope (SEM) coupled with Energy Dispersive X-Ray (EDX) (JEOL JSM6490 LV) was used to analyse the surface of the filter cartridge.

2.4. Experimental plan and calculation methods

As detailed in Table 2, nine experiments were conducted under different system configurations and operational parameters to assess the impact of oxidative HGF on gasification indicators and pollutant content.

Table 2: System configuration, nomenclature and target conditions for all experiments.

System configuration	Test code	$ER_{reactor}$	Secondary air flow rate in HGF unit (NL/h)	ER_{HGF}	ER_{total}	Test duration (h)
Reference	REF (x3)	0.25	0	0	0.25	2

(cyclone)	REF-0.3	0.3	0	0	0.3	2
thermal (HGF without filters)	th-0.05	0.25	910	0.05	0.3	2
HGF (HGF with filters)	HGF-0	0.25	0	0	0.25	4
	HGF-0.05	0.25	910	0.05	0.3	4
	HGF-0.1	0.25	1950	0.1	0.35	4
Cyclone + HGF	cy-HGF-0.05	0.25	910	0.05	0.3	4

First, a series of three reference tests (REF) was carried out under the standard cyclone configuration (depicted in Figure 1) and identical conditions to determine the experimental and analytical uncertainty. Operational parameters inside the gasification reactor, namely: the primary air flow rate, the reactor wall temperature, the primary air-to-feedstock equivalence ratio (ER) and the feedstock throughput, were kept constant at a value of 4500 NL/h, 800°C, 0.25 and 4.5 kg/h (as received), respectively. Results reported for REF test corresponds to the average value calculated from the three repeated tests. Standard deviation values were also included.

Second, the effects of a rise in the ER were determined in the REF-0.3 test under the standard cyclone configuration (see Table 2). For that, the ER inside the reactor was increased from 0.25 to 0.3 by reducing the feedstock throughput from 4.5 to 3.5 kg/h while keeping constant the flowrate of primary air. Therefore, fluidisation regime and residence time inside the reactor were roughly unchanged with respect to the reference tests.

Third, after replacing the cyclone separator by the HGF unit, a thermal test (referred as th-0.05) was conducted by injecting a flow of secondary air into the HGF unit but without any filtration cartridge inside. The aim of the thermal test was to determine the effects of secondary reactions in homogeneous (gas-gas) phase on gasification indicators and pollutant content.

Fourth, three filtration tests were conducted under the HGF configuration by placing two metallic filtration cartridges inside the HGF unit to study the effect of the secondary ER (referred as the ER_{HGF}). The three filtration tests, namely: HGF-0, HGF-0.05 and HGF-0.1, were carried out at

secondary air flow rates values of 0, 1000 and 2000 NL/h, leading to ER_{HGF} values of 0, 0.05 and 0.1, respectively.

Finally, the effect of dust loading in the HGF unit was assessed in the test cy-HGF-0.05 by integrating the cyclone between the reactor and the HGF unit. The duration of all filtration tests was fixed to 4 h in order to amplify dust accumulation on the filter surface. Tar and acid gas sampling were systematically performed during the last 40 min of each test.

The performance of the gasification process was assessed using four output indicators, namely: Low Heating Value (LHV), Gas yield (η_{gas}), Cold Gas Efficiency (CGE) and Carbon Conversion (%C), fully described in the Appendix B. Gasification indicators were calculated excluding the benzene of the composition of the producer gas. Nevertheless, since the presence of benzene in produced gas is not an issue for engine application, gasification indicators were also calculated including benzene in the composition of produced gas and detailed in Table B.1 (Appendix B).

The conversion percentage of tars was calculated according to Equation 1, using the average value determined for the three reference tests as reference value.

$$Conversion, \% = \frac{(\gamma_i - \gamma_{REF})}{\gamma_{REF}} * 100\% \qquad \text{Equation 1}$$

Where γ represents the yield value of each group or molecule (in $g/kg_{feed\ daf}$) quantified in this study.

3. Results and discussion

3.1. System operation and process conditions

Table 3 details the results of the main operation parameters, gasification indicators, gas concentrations and product yields for all experiments conducted in this study. For the sake of clarity, tar yields were specified according to ECN tar classification [34]. The individual yield values of all gas and tar molecules quantified in this study were detailed in Table A.2 (Appendix A). The overall carbon

balance closures were above 80% in all tests, whereas for the hydrogen and oxygen balance closures were between 45-50% and 65-80%, respectively. The low closures values obtained for hydrogen and oxygen can be ascribed to the unquantified water. On the contrary, the deviation in carbon balance can be firstly explained by a numerical artifact that arose from the small variations observed in the instantaneous concentration of CH_4 and CO and the relatively long analytical time of the μ-GC. These variations, that in any case exceeded ± 2 points of the average value, were generated by small fluctuations of the feed throughput. Secondly, it seems that not all carbon could be retrieved since some deposits were formed inside the condensation system. However, the mass of these deposits was negligible compared to the mass of feed used in each test.

Reactor temperature was close to the target value and remained steady for all tests. In the case of the HGF unit, the temperature in both, the dirty side and the gas mixing zone of the HGF unit was roughly consistent between the different filtration tests and close to the set point temperature (450°C). On the contrary, the temperature in the clean side of the filter rose notably for the tests HGF-0.05 and HGF-0.1 leading to values of 523°C and 631°C, respectively. In the case of the test HGF-0.1, the temperature of the clean and dirty side of the HGF showed a progressive and continuous increase after the injection of the secondary air. Latter trend is further discussed in section 3.4.2. Finally, the superficial filtration velocity was kept between 2 and 3 cm/s and residence time of the gas inside the filter ranged between 12 and 16 s for all filtration experiments.

Table 3: Main operation conditions, gasification indicators, gas compositions and product yields for all tests conducted in this study. Relative deviations are presented for the reference tests and corresponds to three separate experiments.

Code of the test	REF	REF-0.3	th-0.05	HGF-0	HGF-0.05	HGF-0.1	Cy-HGF-0.05
Gasifier							
Fuel feed rate, kg/$h_{(as\ received)}$	4.5 ± 0.1	3.5	4.5	4.4	4.5	4.5	4.4
Bed temperature, °C	800 ± 2	805	796	797	797	799	796
Freeboard temperature, °C	757 ± 1	758	761	758	758	759	759
$ER_{reactor}$	0.25 ± 0.01	0.33	0.26	0.26	0.26	0.25	0.26
Hot Gas Filtration unit							
Secondary air feed rate, NL/h	-	-	960	0	960	2040	960
Gas mixing zone temperature, °C	-	-	434	457	435	405	427
Filter temperature, °C (dirty side)	-	-	424	431	431	486	418
Filter temperature, °C (clean side)	-	-	455	453	523	631	465
Face filtration velocity, cm/s	-	-	-	2.3	2.9	3.4	2.8

Gas residence time inside the filter, s	-	-	13.2	16.1	13.8	12.3	13.6
ER_{HGF}	-	-	0.05	0	0.05	0.11	0.06
ER_{total}	0.25 ± 0.01	0.33	0.31	0.26	0.31	0.37	0.32
Gas composition, %mol (N_2-free, dry)							
H_2	17.4 ± 0.6	15.2	15.6	16.8	14.8	14.6	15.5
CO	29.3 ± 0.2	29.1	27.8	28.9	28.7	26.4	28.1
CO_2	39.8 ± 0.4	42.9	39.5	40.1	42.6	47.1	39.9
CH_4	9.1 ± 0.1	8.7	8.3	9.0	8.9	7.8	8.7
C_2H_2	0.33 ± 0.02	0.32	0.29	0.30	0.2	0.05	0.28
C_2H_4	3.0 ± 0.1	2.8	2.8	3.0	2.8	2.5	2.7
C_2H_6	0.36 ± 0.01	0.32	0.34	0.34	0.35	0.29	0.33
C_3H_4	0.04 ± 0.004	0.03	0.03	0.04	0.03	0.01	0.04
C_3H_6	0.29 ± 0.04	0.25	0.28	0.37	0.29	0.19	0.29
O_2	0.4 ± 0.2	0.4	5.1	1.2	1.4	1.0	4.3
Gasification indicators							
Gas Yield, $Nm_3/kg_{feed\ (daf)}$	1.78 ± 0.05	2.26	2.06	1.86	2.09	2.32	2.13
Gas Yield, $Nm_3/kg_{feed\ (daf)}$, (N_2-free)	0.65 ± 0.01	0.72	0.70	0.71	0.74	0.77	0.74
LHV, MJ/Nm^3	5.4 ± 0.1	4.7	4.6	5.4	4.7	3.9	4.7
%CGE	44.3 ± 0.02	48.4	44.7	46.0	46.2	43.4	46.8
%C	58.1 ± 0.02	67.9	61.3	62.0	65.7	66.7	64.2
%H	48.0 ± 0.02	50.3	47.9	50.4	49.0	46.4	50.1
Tar yield[a], $g/kg_{feed\ (daf)}$							
benzene	6.2 ± 0.1	7.7	7.0	6.9	6.9	7.2	6.0
Class II	0.61 ± 0.11	0.53	0.48	0.55	0.31	0.24	0.41
Class III	5.5 ± 0.2	6.3	5.6	6.0	4.9	2.7	4.8
Class IV	5.1 ± 0.4	5.4	4.3	6.4	4.3	2.7	4.3
Class V	0.31 ± 0.04	0.33	0.30	0.43	0.23	0.19	0.22
Total[b]	11.6 ± 0.2	12.5	10.8	13.4	9.8	5.9	9.7
Gas dew point[c], °C	173	170	164	174	164	163	165
Volume gas sampled tar protocol, NL	~60	60.71	58.25	57.38	57.07	54.72	56.13
Water and acid gas yield, $g/kg_{feed\ (daf)}$							
NH_3	18.5 ± 4.9	24.2	11.3	16.3	25.9	20.2	23.4
HCN	2.5 ± 0.3	3.5	1.5	3.2	1.0	0.2	2.0
H_2O	341 ± 13	347	348	308	331	346	338

[a]tar groups according to the ECN tar classification. [b]Total tar yield is expressed on benzene-free basis.

[c]Calculated using the complete model developed by ECN (www.thersites.nl)

3.2. Balances and characterization of products for Reference tests

Gas composition and gasification indicators values obtained for the reference tests (REF) are in line with values typically reported in literature [35,36]. The total tar yield resulted in 1.16 wt.% (daf feedstock basis), which corresponds to a concentration of 10.0 g/Nm^3 (dry gas) or 6.5 g/Nm^3 (dry gas, C_6H_6-free). The tar composition was in line with results typically reported for fluidized bed gasification reactors and similar gasification conditions [37]. Water content of producer gas, estimated from the hydrogen balance, resulted in a concentration value of approximatively 13.5 wt.% (wet gas), which compare well with water content values typically reported for bubbling bed gasification of relatively dry feedstocks [37]. Oxygen balance closures, re-calculated on wet basis, led

to values in a range between 95-100%, indicating a relatively good accuracy of the indirect water quantification method.

Figure 4 reproduces the SF spectra (recorded with a Δλ of 3 and 20 nm) corresponding to the tar protocol samples of the three REF tests. The overlapping of the SF spectra indicated a close chemical composition between the REF samples, as well as, an excellent experimental and analytical repeatability. Thereafter, and for the sake of clarity, only one of the three REF spectra was shown in the SF figures. Moreover, it is well known that the emission wavelength band on the SF spectrum can be correlated to the number of the aromatic rings, in particular, for linear PAHs [38–43]. According to Kister et al.[29], molecules having 2-3 linearly condensed aromatic rings (PAHs with one naphthalene skeleton) show a SF signal in a spectral range between 300-370 nm while, molecules having 3-4 linearly condensed aromatic rings (PAHs with one anthracene or benzofluoranthene skeleton) show a SF signal in a spectral range between 370-460 nm and, molecules having four or more linearly condensed aromatic rings (PAHs with one tetracene or benzofluoranthene skeleton) show a SF signal in a spectral range between 460-580 nm. Based on Kister's assignment and in excellent agreement with the results of quantitative chemical analysis, SF spectra revealed a chemical composition of REF samples dominated by PAHs with 2 to 3 linearly condensed rings and their derivatives. Furthermore, the relation between the emission wavelength band and the number of aromatic rings of the PAH molecules present in REF samples was confirmed by the spectral ranges obtained for aromatics and PAHs model molecules. As seen from Figure 4, the light tars molecules with 1-2 aromatic rings present a spectral band between 250 and 320 nm whereas, heavier tar molecules having 3-4 aromatic rings present a spectral band from 320 to 400 nm. Moreover, as evident from Figure 4, spectra of model molecules at Δλ=20 nm exhibits a better segregation vs. their molecular size and, propanol does not present a signal (compared to the marked signal observed at Δλ=3 nm). Accordingly, SF spectra recorded at Δλ=20 nm were used in this study.

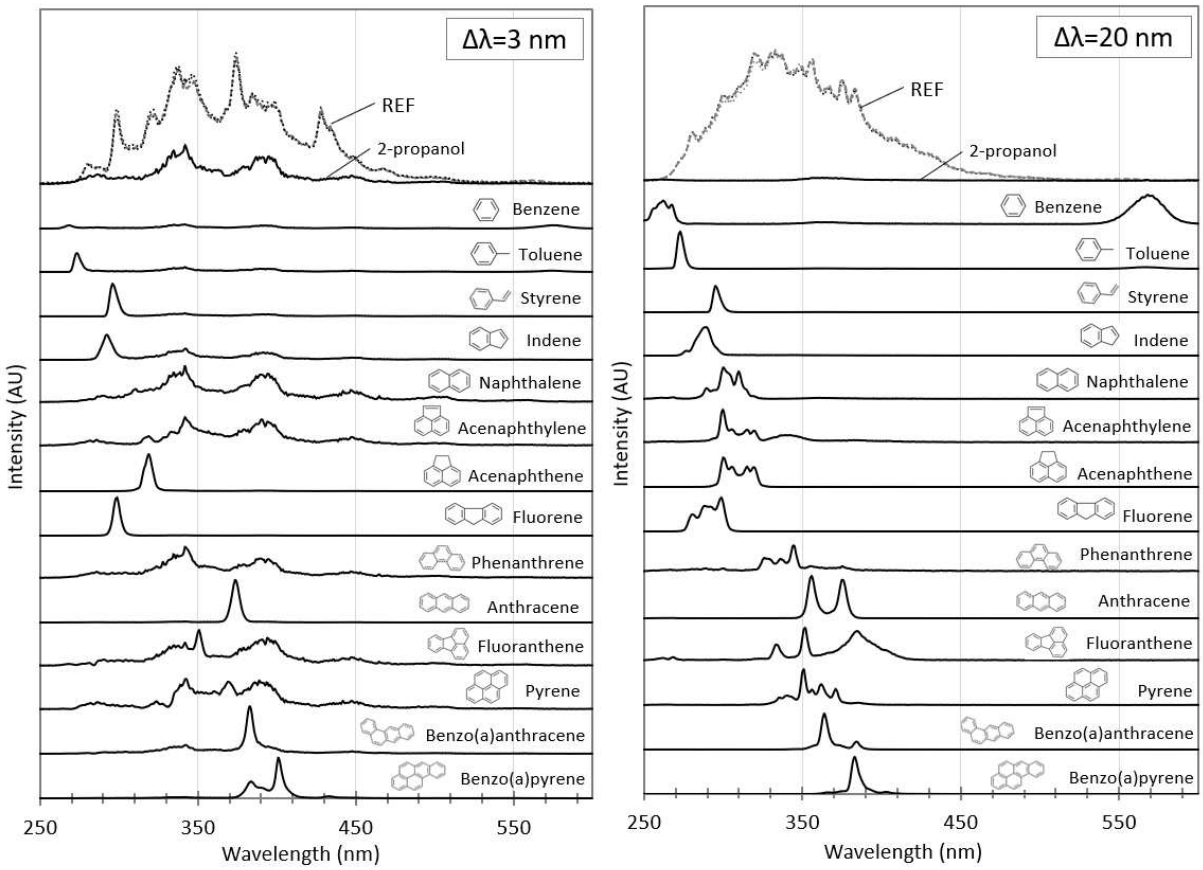

Figure 4: Synchronous Fluorescence spectra recorded at offset=3 nm (left) and offset=20 nm (right) of three reference experiments, 2-propanol and 14 model molecules.

The yields of NH_3 and HCN for the REF test were 18 g/$kg_{feed(daf)}$ and 2.5 g/$kg_{feed(daf)}$, which correspond to concentration values of 10.1 g/Nm^3(dry gas) and 1.4 g/Nm^3(dry gas), respectively. Nitrogen partitioning, determined from the results of the nitrogen balance (Table 4), indicated that 43% of the Fuel Bounded Nitrogen (FBN) was converted to NH_3 and 4% to HCN. The char bounded nitrogen (N-char), calculated from elemental analysis of the char recovered from the reactor, the cyclone and the filter, was about 5% whereas, the tar bounded nitrogen (N-tar) was neglected because nitrogen containing species were not detected by GC-MS/FID analysis. These results were close to partitioning values reported for the gasification of N-rich biomass feedstocks [44,45]. The slight divergences can be ascribed to the different nature of the FBN. For instance, in raw lignocellulosic biomasses, nitrogen bearing species are intrinsically bounded to the molecular structure of the plant. In contrast, in MDF materials, nitrogen is mainly contained in the resin used to stick the wood fibres of the composite. Therefore, thermal decomposition mechanisms of nitrogen bearing species contained in

MDF might differs to those observed for raw lignocellulosic biomasses, impacting thus, the FBN partitioning results. Moreover, the N_2 generated by the gasification reaction was determined by difference since it was not possible to distinguish it from the total N_2. Indeed, it is likely that nitrogen oxides (NO_x) were also present because these molecules are typical products of the combustion of N-containing fuels [46,47]. On that basis, the results showed that approximatively 47% of the FBN was converted to N_2 and NO_x. Finally, the error induced by the addition of the N_2 derived from the FBN to the flow of total N_2 was marginal since the instantaneous flow rate of the former represents less than 1% of the instantaneous flow rate of the latter.

Table 4: Nitrogen repartition balance (%). N_2+NO_x values were calculated by difference. Quantified % represents the mass ratio between the nitrogen initially present in the biomass and the nitrogen quantified in NH_3, HCN and char.

	REF	REF-0.3	th-0.05	HGF-0	HGF-0.05	HGF-0.1	Cy-HGF-0.05
NH3	44 ± 11	56	27	40	64	50	56
HCN	3.9 ± 0.6	5.1	2.2	5.0	1.6	0.3	3.0
Char	5 ± 2	5	6	14	6	8	4
N2+NOx	47 ± 13	34	65	41	29	42	37
% quantified	52	66	35	59	71	58	63

3.3. Thermal experiments: Effects of ER on indicators and products

In line with previous studies[48,49], the increase in the ER (from 0.25 to 0.3, see Table 2) of the gasification reactor operated for the test REF-0.3 led to a rise in the gas yield, CGE, %C and %H and a drop in LHV (see Table 3). The chemical analysis of tar samples showed only a slight increment in overall tar yield, mostly due to a rise in the yield of benzene and tars of class III (in particular of toluene, phenylethyne, styrene and indene), while class IV and V remained unchanged. The lack of major variations on tar yields can be ascribed to the fact that the temperature in bed and freeboard zone of the reactor was roughly unchanged with respect to the REF tests. The SF spectra, depicted in Figure 5, did not show any marked difference in the spectral fingerprint between the REF-0.3 and REF samples (at ER=0.25). The slight decrease in the spectrum intensity can be ascribed to the reduction in the feed throughput operated for the test REF-0.3. Finally, the increase of the ER did not show a significant impact on the water yield

whereas, the yields of NH_3 and HCN rose of 33% and 36%, respectively. These results are in line with the results reported by Broer and Brown [50], and confirms that the higher the ER inside of the reactor, the more NH_3 and HCN are released from the feedstock material.

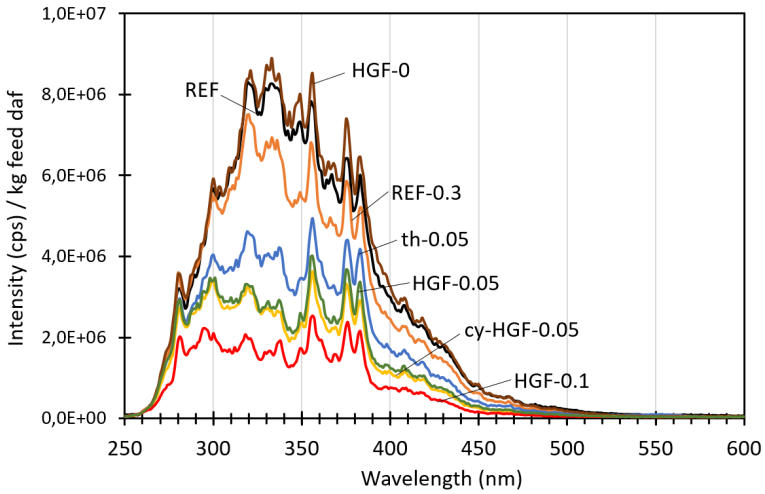

Figure 5: Synchronous Fluorescence spectra (Δλ=20 nm) of all experiments.

Compared to the reference test (REF), the results obtained for the test th-0.05, conducted by injecting a flow of secondary air into the HGF unit but without filtration cartridges, showed a slight increase on the gas and carbon yield and a drop on the LHV. The average oxygen concentration measured during the test th-0.05 dropped with respect to the theorical oxygen concentration obtained in the absence of secondary reactions, estimated to 7.5%vol (N_2-free dry gas). As already reported by Jiang et al.[51], the oxidation reactions of main combustible gas species contained in the producer gas starts above 450°C while, the oxidation of solid dust particles was reported to start as low as 150°C. During the test th-0.05, the temperature of the producer gas at the entrance of the gas mixing zone inside the HGF unit was about 460°C. Therefore, it is likely that partial oxidation reactions of combustible permanent gases (H_2, CO, CH_4) and fine carbon-rich dust particles arriving to the HGF took place to some extent, explaining the decrease in the LHV and slight increase observed in the carbon yield.

Regarding the chemical analysis of tar, and despite the fact that the overall tar yield resulted unchanged, our results indicated a slight increase in the yield of benzene, toluene and benzofuran

and a drop of 50% in the phenol yield, while the light and heavy tars of class IV and V remained globally unchanged (within experimental uncertainty). The drop in the yield of phenol and the increase in more stable aromatics (benzene) has been already pointed out as a consequence of staged injection of air [52]. The SF spectrum of the th-0.05 sample (Figure 5) did not revealed marked differences in the spectral fingerprint compared to REF sample, supporting the marginal effect on light and heavy tars observed by quantitative analysis. By contrast, the drop in the overall intensity of the spectrum indicated that producer gas dilution (as a result of the secondary air injection) impacted the PAHs concentration in the gas flow. In conclusion, and consistent with thermal cracking literature [53,54], these results provide evidence that mild temperature inside the HGF unit was too low to activate the cracking reactions of refractive light and heavy PAHs. Finally, the yields of NH_3 and HCN dropped of 38% and 43%, respectively. The drop in NH_3 can be ascribed to oxidation reactions in homogeneous phase as these reactions can be initiated at about 427°C [55]. On the contrary, oxidation reactions of HCN are known to take place at higher temperatures (>700°C) but, they can be catalysed by the presence of some permanent gases (CO, CH_4) and the extended residence time inside the filter [56].

3.4. Filtration experiments

3.4.1. Impact of oxidative HGF: homogeneous vs. heterogeneous secondary reactions

Secondary reactions inside an oxidative HGF unit can undergo through homogeneous (gas-gas) and heterogeneous (gas-solid) reactional pathways. In the former case, the results obtained for the thermal test (th-0.05) evidenced that, in spite of the mild temperature, partial oxidation reactions in homogeneous phase took place to some extent impacting significantly the %C and LHV but, with little effect on the yield of light and heavy tars. In the latter case, secondary heterogeneous reactions are expected to result from the interaction between the syngas and either the dust cake particles, or the dense non-woven metal fibre layer of the filter, or both simultaneously. Thus, to isolate the effects of secondary heterogeneous reactions, the results of the test HGF-0.05 were compared with those of

455 the test th-0.05 indicating, as seen from Table 3, an increase of 3%, 7% and 2% in the CGE, carbon
456 and hydrogen yields.

457 Regarding the chemical composition of tars, results showed a drop of 10% on the overall tar yield
458 between the tests th-0.05 and HGF-0.05, mainly due to the reduction of tars of class II, III and V. In
459 the case of aromatics of class II and III, the most market drop was observed on phenol and
460 phenylethyne yields, showing a decrease of 36% and 12%, respectively. The unchanged value
461 observed in the yield of tars of group IV can be ascribed to opposite trends between acenaphthylene
462 (which yield increased by 12%) and the rest of the group (see Table A2, Appendix A). Moreover, the
463 drop in the overall SF spectrum intensity observed between the HGF-0.05 and th-0.05 samples
464 (Figure 5) corroborate the reduction observed by quantitative analysis.

465 Finally, the yields of water and HCN were unchanged with respect to th-0.05 (within experimental
466 uncertainty) whereas, the yield of NH_3 rose by 129%. A possible explanation for the substantial
467 increase in the yield of NH_3 is the release of NH_3 from dust cake particles as a result of partial
468 oxidation reactions. Indeed, the rise of 90°C observed between the temperature of the clean and
469 dirty side of the filter during the test HGF-0.05 and the increase in the carbon yield evidenced that
470 exothermic partial oxidation reactions happened on the filter surface. Therefore, N-containing
471 species in solid (N-char) and, to a lesser extent aerosol (N-tar), phases arriving to the filter were likely
472 converted to NH_3. Consistent with latter hypothesis, the fraction of quantified N-species (see Table 4)
473 showed its highest value for the test HGF-0.05.

474

475 ### 3.4.2. Impact of secondary air on the operation of the HGF unit

476 The impact of secondary air flow rate was assessed based on the results of the three filtration tests,
477 namely: HGF-0, HGF-0.05 and HGF-0.1. These tests were conducted with the same set of filter
478 cartridges following the next order: 1st) HGF-0.05, 2nd) HGF-0 and, 3rd) HGF-0.1. In each of the three

tests, a dust cake of approximatively 10-20 mm thickness was accumulated on the filter surface. In the case of the tests HGF-0.05 and HGF-0, the dust cake was loosely adhered to the filter surface and fell off spontaneously during the off-line cleaning operations. On the contrary, for the test HGF-0.1, the dust cake was more stable and did not fall off easily (Figure 6).

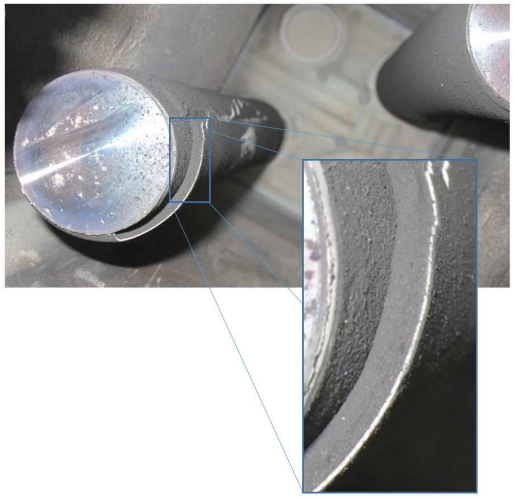

Figure 6: Photograph of the dirty side of the HGF unit after the test HGF-0.1

Figure 7 depicts the differential pressure across the filter for all filtration tests and the temperature profiles measured inside the HGF unit during the test HGF-0.1. The lack of exhaustive cleaning of filter surface before the tests HGF-0 and HGF-0.1 explains the rapid rise in the pressure drop at the beginning of these tests in comparison with the smooth increase observed for the test HGF-0.05. Regarding the long-term trends, results showed a similar rate of pressure drop increase during the tests HGF-0.05 and HGF-0 that contrast with the change in the slope observed for the test HGF-0.1 beyond 2 h. The sharp change in the slope was caused by the formation of a low permeability ash layer on the filter surface as a result of the presence of excess amount of oxygen and the higher temperature. Indeed, 2 h after the start of the test HGF-0.1, the temperature of the clean side of the filter was 145°C higher than the temperature on the dirty side (see Table 3) clearly indicating that dust cake particles were oxidised to a large extent. The presence of ash deposits on the dust cake was confirmed by visual inspection after the test HGF-0.1 (Figure 6).

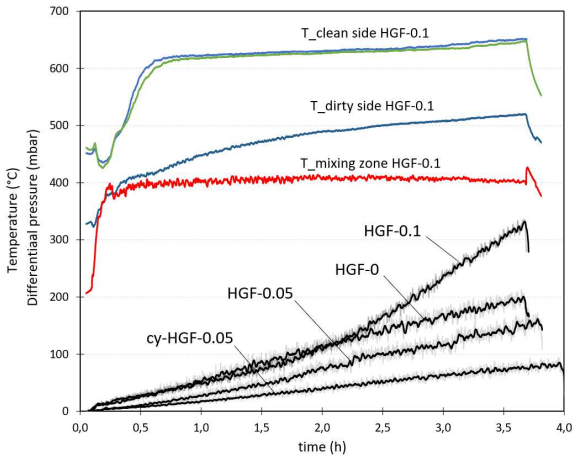

Figure 7: Temperatures inside the HGF unit during the test HGF-0.1 and pressure drop across the filter for the tests: HGF-0, HGF-0.05, HGF-0.1 and cy-HGF-0.05.

To gain further insight on the state of the outer filter surface, several samples of the filter mesh (approximate size of 1-2 cm^2) were carefully extracted from the lower, medium and upper part of the filter and analysed by SEM-EDX (Figure 8A-D). To be noted that prior to sample extraction, the remaining dust cake was dislodged by gentle shaking and vacuum aspiration.

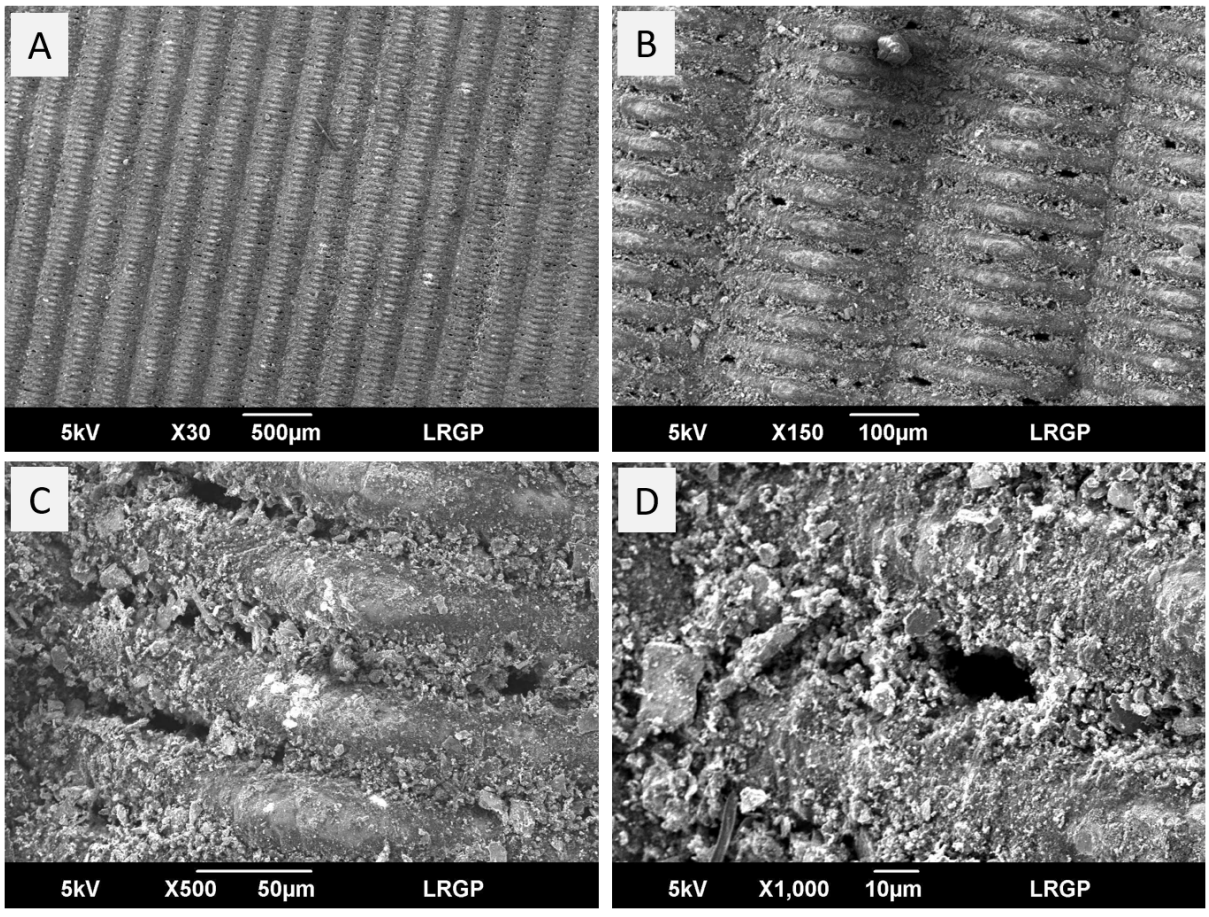

Figure 8: SEM images of the surface of the dirty side of the filter cartridge after the test HGF-0.1.

As evident from Figure 8A-D, slagging, sintering and aggregation phenomena between the particles deposited in the inter-wire space of the outer filtration membrane took place, blocking the porosity and thus, reducing drastically the filter permeability. Based on particle morphology shown in Fig.8C-D, deposits mainly consisted on: (a) discrete angular sharp micro-particles of olivine and, (b) micron- and sub-micron residual ash particles of irregular shape. Additionally, as seen in Fig.8D, an ash layer was developed on the surface of the metallic wires. This sticky layer is known to favour the pick-up of micro-particles and inorganics [57].

To reveal the nature of the ash deposits formed in the porosity of the filter, EDX spot analyses were conducted in several characteristics points of the filter surface. Spot location and the estimated elemental composition of each spot were detailed in Figure 9.

Figure 9: SEM-EDX spot analysis of the dirty side of the filter cartridge after the test HGF-0.1. Yellow crosses show the points (spots) where the EDX analysis was carry out. Estimated elemental composition is expressed in mass basis.

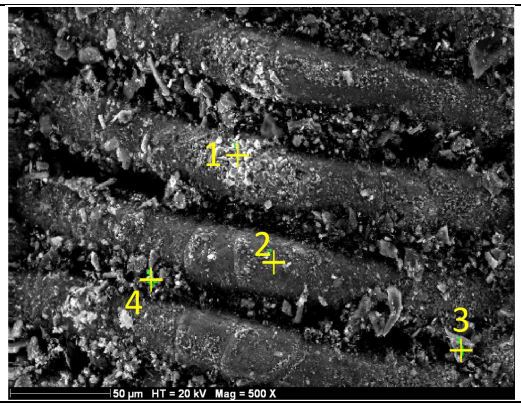

	wt.% (by EDX)			
Element	**Spot 1**	**Spot 2**	**Spot 3**	**Spot 4**
C	4.61	11.64	36.01	31.92
O	41.46	21.18	31.85	38.3
Mg	0.31	0.21	16.53	13.19
Al	38.51	0.15	0.04	0.43
Si	0	0.54	11.4	8.47
Cr	3.04	12.31	0.31	0.32
Fe	10.43	48.21	3.38	5.15
Ni	1.54	4.21	0	0
P	0	0.16	0	0.27
S	0	0.77	0	0
K	0	0	0.42	0.34
Ca	0	0	0	1.47
Mn	0.11	0.62	0.05	0.13

According to the EDX analysis of spot 4, the ash deposit accumulated on the inter-wire space of the outer membrane was primarily composed of: K, Ca, P, O, C, Mg, Si and Fe. Strictly considering the ash melting temperatures determined for the parent feedstock particles (Table 1), melting phenomena was not expected to take place on the dust cake because maximal temperature measured inside the HGF unit during this study was 630°C. However, SEM observations evidenced sintering and

aggregation of ash particles in the inter-wire space of the filter. Therefore, and taking into account the complex phase chemistry of multicomponent ashes, the formation of consolidated ash deposits likely resulted from the combination several factors, such as: (i) the occurrence of high temperature spots resulting from the exothermal oxidation of carbon-rich dust particles, (ii) alkali melting on the surface of olivine micro-particles elutriated from the reactor and deposed on the filter surface, (iii) the small particle size and, (iv) the elevated residence time [57–60]. Notably, the softening temperature measured in Table 1 is associated to the softening of the ashes as mainly oxide species. Elutriated particles from the fluidized bed are still rich in carbon which can enhance their carbo-reduction. Furthermore, the reduction of metal species present in the carbon-rich ashes may be further promoted by the producer gas (rich in CO, H_2, etc.). It is known that an increased mobility of the metallic species occurs near their Tammann temperature, which is defined as the temperature that lies in the range 0.3 to 0.5 times the melting point [61]. All these phenomena can explain a so low temperature of agglomerate formations compared to the high temperature of ashes softening measured by the common normalised test.

Alkali melting on the surface of olivine particles was confirmed by EDX analysis of spot 3. As seen from Figure 9, spot 3 corresponds to a discrete and angular sharp particle containing Mg, Si, O and Fe, which are known to be the main chemical elements of olivine. High amount of K detected in spot 3 suggests the formation of K-bearing species on the surface of the olivine particle. The low melting points of K-bearing species and the propensity of these species to form low melting eutectics in between K-bearing species and/or with other mineral phases have been already reported [62,63]. This phenomenon promotes the irreversible aggregation of particles of ash and olivine.

Finally, the elemental composition of spot 1 indicated a high content of aluminium and oxygen. From a morphological point of view, these deposits did not appear to be originated through the same mechanisms detailed previously for the deposition of ash. Instead, these deposits were likely

549 originated from the alumina-rich product used during the assembling fabrication process of the
550 filtration mesh. The aluminium oxide deposit was also identified in specific locations of the clean side
551 of the filter (see Figure A.1, Appendix A).

552 The SEM-EDX results clearly present that increasing the secondary air flow rate leads to the
553 formation of ashy deposits, reducing the permeability of the filter. Irreversible character of ash
554 deposition mechanisms (aggregation, melting, sintering) is expected to reduce efficiency of back
555 pulse cleaning. Therefore, secondary air flow rate must be selected in order to limit the extent of
556 oxidation reactions. Based on the results described above, an ER_{HGF}=0.05 represent a good trade-off
557 between reactivity and stability of the filtration operation for a dust particle mass flow rate entering
558 into the filter of ca. 120 g/h and mild filtration temperatures. To be noted that the ER_{HGF}=0.05 was
559 calculated based on the feedstock composition and throughput. Alternatively, the ER_{HGF} can be also
560 calculated based on the composition and volumetric flow rate of the producer gas entering into the
561 filter, leading to values of 0.15 and 0.30 for the tests HGF-0.05 and HGF-0.1, respectively.

562 ### 3.4.3. Impact of secondary air on the gasification indicators and products

563 Compared with the reference test (REF), gasification indicators values obtained for tests HGF-0, HGF-
564 0.05 and HGF-0.1 revealed that an increase in the secondary air flow rate inside the HGF unit lead to
565 a rise in the gas yield and %C and, a drop in the %H and LHV. The CGE slightly increased for the tests
566 HGF-0 and HGF-0.05 and, decreased for the test HGF-0.1. Variations on gasification indicators mainly
567 stem from the rise in the yield of CO_2 and the drop in the yield of C_2H_2, C_3H_4 and C_3H_6 (see Table A.2,
568 Appendix A) since, for the rest of the gases, no clear trend emerged within the experimental
569 uncertainty. The reduction in the yield of C_2-C_3 hydrocarbons, in comparison with the unchanged
570 yield of CH_4, may be explained by the lower stability of C_2-C_3 molecules, compared to CH_4.

571 The chemical analysis of tars showed a drastic decrease in the overall tar yield with increasing flow
572 rate of secondary air. Thus, for test HGF-0.1, the overall tar yield dropped as much as 49% with
573 respect to the REF test (see Table 3). In this instance, the yield of tar groups of class II and III dropped

574 of 60% and 51% whereas, the decrease of class IV and V was of 46% and 37%, respectively. Latter
575 trends were corroborated by the SFS results plotted in Figure 5. In contrast to the REF sample, the SF
576 spectrum of the HGF-0.1 sample showed a decrease in the overall intensity and a shift to lower
577 wavelengths, indicating a reduction in the content of heavy PAHs molecules.

578 Moreover, the yield of water and HCN showed a decreasing trend with the increase in the secondary
579 air flow whereas, the yield of NH_3 peaked for the test HGF-0.05 and then decreased with increasing
580 secondary air flow rate. A possible explanation of the variation observed in NH_3 and HCN is the
581 occurrence of simultaneous releasing-abatement mechanisms inside the HGF unit. Thus, on the one
582 hand, the more severe oxidation of dust cake particles increases the amount of NH_3 and HCN
583 released to the gas. In the other hand, the abatement reactions undergo through homogeneous and
584 heterogeneous pathways as a result of the excess presence of oxygen and the elevate temperature.
585 However, from the data available it is difficult to unveil the precise mechanism because of the lack of
586 NO_x quantification. Therefore, in future research dealing with the fate of N-containing species from
587 air-blown gasification it is advised to quantify NO_x species, as well as, the use of another μ-GC tracer
588 gas different than N_2.

589 Finally, it is interesting to note the increase of 16% in the overall tar yield of the test HGF-0 with
590 respect to the REF test, primarily caused by the rise in the yields of light and heavy tars of class IV and
591 V by 27% and 29%, respectively. In terms of individual yields, the most marked variation corresponds
592 to pyrene, showing a rise of 53%. These unexpected results are supported by the slight increase in
593 the intensity of the SF spectrum for the HGF-0 sample within a wavelength range of 330-400 nm (see
594 Figure 5). Moreover, the yield of major gas compounds did not change notably with respect to the
595 reference values, only propylene showed a rise of 26% on its yield. Regarding on-line gas
596 concentrations, only propylene and acetylene showed slight downward trends during the test HGF-0.

597 As pointed out in [64], the catalytic cracking of substituted aromatics on the surface of char particles
598 leads to the formation of larger PAHs molecules, probably via phenyl radical intermediates.

599 Nevertheless, these reactions are known to initiate above 600°C and become significant at 800°C[65].
600 In this study, temperature inside the filter during the test HGF-0 was kept between 430°C and 450°C.
601 Thus, catalytic cracking of substituted tars molecules was not expected to take place on the surface
602 of dust particles. A possible explanation for the slight increase observed in the yield of tars of class IV
603 and V is the gasification of carbon-rich dust cake particles by reactive gaseous species of the
604 producer gas, in particularly: CO_2 and H_2O. These reactions are known to take place at higher
605 temperatures but, they can be catalysed by the small particle size and the high inorganic content of
606 dust cake particles [20,66]. Consistent with latter hypothesis, Ravenni and co-workers[64] reported
607 upwards trends for naphthalene, anthracene and pyrene molecules during the catalytic cracking of a
608 real producer gas with a bed of char particles kept at 800°C. Considering similarities between the
609 spatial velocities (7.2 NL/g_{char}.h in [64] and, 9.7 NL/g_{char}.h in this study) and water content of producer
610 gas 10-15 %(v/v), greater production values obtained in [64] for these molecules must have been
611 caused by the gap of more than 300°C in the cracking temperature between these two studies.

612 ### 3.4.4. Impact of dust loading on the operation of the HGF unit

613 As expected, the integration of the cyclone separator between the gasification reactor and the HGF
614 unit operated for the test cy-HGF-0.05 lead to a notable reduction of the mass of dust accumulated
615 on the filter. The mass yield of the dust cake recovered after the test cy-HGF-0.05 was 0.7 wt.%, far
616 below the 3.7 wt.% estimated for the test HGF-0.05. Visual inspection of the filter after the test cy-
617 HGF-0.05 revealed a dust cake about 5-10 mm thickness, composed of very fine particles without any
618 apparent sign of ash formation (see figure A.2, Appendix A). In this case, the dust cake did not fall
619 spontaneously during off-line cleaning operation and thus, could be entirely recovered. Pressure-
620 drop profile of the test cy-HGF-0.05, shown in Figure 7, evidenced that integrating the cyclone led to
621 a reduction of the rise in the pressure drop. Finally, temperatures inside the HGF unit during the test
622 cy-HGF-0.05 were close to those measured for the thermal test (th-0.05) with the exception of the
623 10°C gap observed between the clean and dirty side the filter.

The morphology and composition of dust particles accumulated on the outer filter surface were assessed by SEM-EDX analyses of a sample of metallic mesh extracted following the procedure beforehand detailed. As seen from Figure 10A-D, the outer surface of the filter was rather pristine and only minor dust deposits were observed. From a morphology point of view, dust deposits were mainly composed of discrete particles with irregular shapes agglomerated in disperse clusters. Dust particles appeared to be loosened adhered to the surface of the metallic wires and no signs of interparticle aggregation were observed. Olivine particles were almost non-existent.

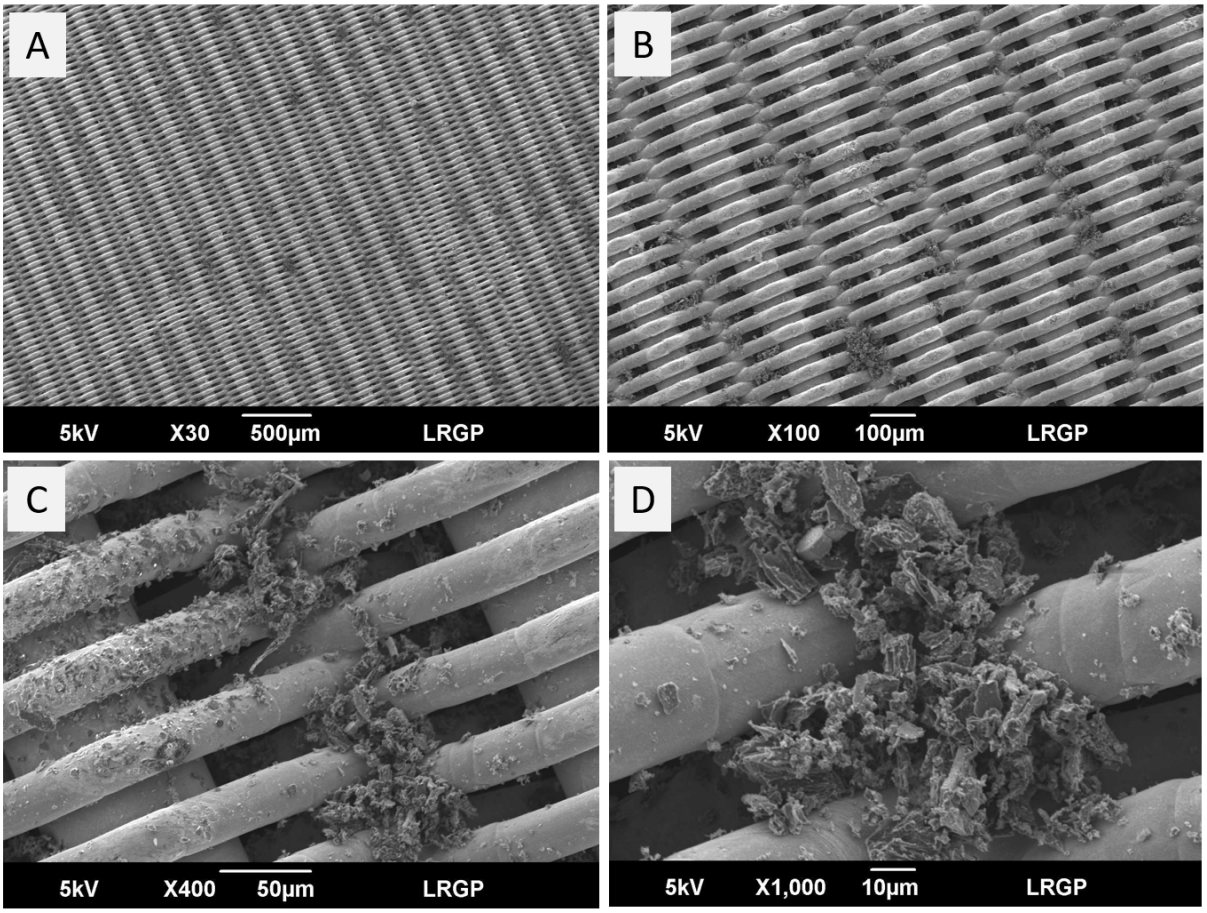

Figure 10: SEM images at different magnification of the surface of the dirty side of the filter cartridge after the test cy-HGF-0.05

Moreover, elemental composition of dust particles recovered from the cyclone and the filter dust cake after the test cy-HGF-0.05 was compared in Table 5. Results showed a lower carbon and higher nitrogen content for the filter dust cake particles. The presence of a considerable amount of olivine

particles in the cyclone sample resulted in ash contents greater than 50 wt.%, which prevent an accurate comparison to be made. Instead, ash content of cyclone particles was supposed to be equal to the ash content measured for the char particles recovered from the reactor after the test cy-HGF-0.05. In this instance, particles of char could be easily isolated from olivine by manual mesh sieving because of the marked difference in particle size. Keeping in mind this latter approximation, results indicated a marked increase of the ash content for the filter dust cake particles. In line with these results, ICP-AES quantification showed a significant enrichment in the content of alkaline (Na, K), alkaline earth (Ca), P and Mn for the filter dust cake particles. The results obtained for Mg, Fe and Si were not examined because of the possible presence of olivine particles in the samples. Several reasons can explain the higher inorganic content of the filter dust cake particles, such as: (i) the tendency of inorganic material to concentrate in the lower particle size fraction of the ground lignocellulosic feedstock and thus, of the char particles[67], (ii) the enrichment in volatile inorganics through condensation/agglomeration mechanisms catalysed by extended exposition to producer gas[60] and, (iii) the partial oxidation of dust cake particles as a result of extended residence time, suitable temperatures (400-500°C) and the presence of O_2 [19].

Table 5: Analysis of cyclone and filter cake particles recovered after the test cy-HGF-0.05. Note that ash content of cyclone particles was estimated from the ash content of the char particles remaining in the reactor.

sample	Cyclone particles	Dust cake particles
Ash*, wt.%(as received)*	1.5 ± 0.1	16.4 ± 1.7
Ultimate analysis, wt.% (as received)		
C	76.7 ± 1.1	60.0 ± 0.8
H	1.04 ± 0.03	1.4 ± 0.1
N	3.1 ± 0.1	8.2 ± 0.5
$O_{calculated\ by\ difference}$	17.6 ± 1	13.9 ± 0.3
Metallic element analysis (mg/kg, db)		
Si	113550 ± 3700	31260 ± 17800
Mg	164590 ± 21400	28670 ± 3200
Ca	5370 ± 230	30000 ± 2670
K	4900 ± 100	9570 ± 580
Na	530 ± 22	880 ± 58
P	534 ± 4	4200 ± 140
Al	4990 ± 2950	1280 ± 910
Fe	27770 ± 1560	5940 ± 600
Zn	41 ± 1	1450 ± 1600
Mn	790 ± 100	3330 ± 45

From an engineering view point, lack of aggregation, sintering and melting phenomena on the filter surface are key features to assure long-term operation of HGF units. Indeed, mild filtration temperature and controlled concentration of O_2 limited the extent of oxidation reactions of the dust cake particles and thus, the formation of high temperature spots on the filter surface, preventing the irreversible blocking of the filter porosity by aforementioned mechanisms. On the other hand, as clearly evidenced in Figure 10C-D, dust micro-particles penetrate the outer filter membrane and were retained by the second layer composed of non-woven metallic fibres. Although, penetration of sub-layers by micron and submicron particles is generally identified as a negative phenomenon regarding the filter lifespan, for example in ceramic candles [19], the open structure of the outer layer of the metallic cartridges used in this study is likely to have a positive effect on the removal of these particles by back-pulse cleaning and thus, preserve long-term filter permeability. Furthermore, extended lifespan and total recyclability of metallic cartridges could compensate the higher cost of metallic elements in comparison to ceramic candles. However, it is noteworthy that the time-on-stream of the set of filter cartridges used for the test cy-HGF-0.05 was limited to 4 h and therefore, complementary experiments are required to further explore the long-term behaviour.

Furthermore, results detailed on Table 5 support the idea that properties of cyclone and dust cake particles have the potential to be in compliance with the limits indicated by the European Biochar Certificate for application as EBC-Agro biochar of class III [68]. Indeed, both cyclone and dust cake particles fulfil thresholds values for properties such as: organic carbon content, H/C and O/C ratios and heavy metal content. Concerning PAH content, only dust cake particles appear to comply with EBC's limit values. Latter conclusion was inferred from the comparison of the SF spectra of liquid extracts from particle samples collected from the cyclone and the filter dust cake after the test cy-HGF-0.05 (Figure 11). In line with the results reported by [64], the release of PAH molecules from char particles is strongly reduced after the exposition of these particles to reducing/oxidizing atmospheres at mild-to-high temperature for long periods of time. This reduction would be linked to the stabilisation effect of secondary carbon deposition, oxidation and/or gasification reactions on the

surface of the char particles. However, it should be noted that analytical methods employed in this study for char characterization differ slightly from those reported on the EBC's guidelines. Thus, complementary analyses, including PAH quantification, are required to draw an accurate conclusion.

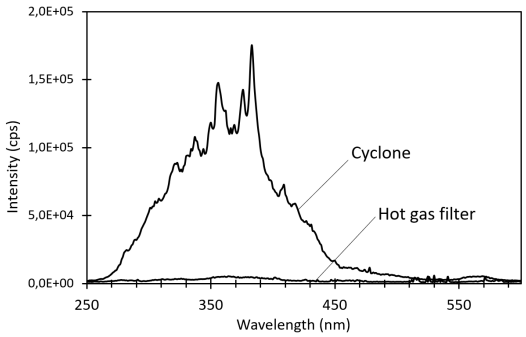

Figure 11: Synchronous Fluorescence spectra (Δλ =20 nm) of 2-propanol extracts of the cyclone and dust cake particles recovered after the test cy-HGF-0.05.

3.4.5. Impact of dust loading on gasification indicators and products

Gasification indicators values obtained for the test cy-HGF-0.05 were close to those obtained for the test HGF-0.05. The average concentration of O_2 measured during the test cy-HGF-0.05 was higher than the concentration measured during the test HGF-0.05 and close to the concentration measured during the test th-0.05, indicating that partial oxidation reactions took place but to a small extent. It appears that the dust particle flow rate entering into the filter (estimated to 30 g/h) was too low to impact significantly oxygen concentration.

The overall tar yield obtained for the test cy-HGF-0.05 was roughly identical to that obtained for the test HGF-0.05. Lack of major deviations on the overall tar composition was confirmed by the overlapping of SF spectra between HGF-0.05 and cy-HGF-0.05 samples (see Figure 5). In terms of individual compound yields, the decrease in the dust loading only impacted significantly the yield of phenol, reducing it conversion from 50%, in the case of the test HGF-0.05, to 32% in the case of the test cy-HGF-0.05. Moreover, slight variations were also observed on other tar compounds with respect to the test HGF-0.05 but no conclusion could be made within experimental uncertainty. Overall, these results suggest that secondary heterogeneous reactions inside the HGF unit arose

mainly from the interaction between the tar molecules transported in the gas phase and the dense non-woven metal fibre layer of the filter. Therefore, the thickness of the dust cake had only a minor impact on the gasification output indicators and tar content. Latter observation could be ascribed to the high porosity of the filter cake and the low probability of interaction between the dust cake particles and the tar molecules transported in the gas phase.

Finally, compared with the test HGF-0.05, the yield of HCN and H_2O did not differ significantly whereas, in the case of NH_3, the production percentage decrease from 43% to 29% with the reduction of the dust loading. Lower production of NH_3 observed with the reduction of dust loading confirmed the release mechanism previously proposed as a result of the partial oxidation of dust cake particles.

4. Conclusion

The present study examines the effect of oxidative HGF on the gasification indicators and pollutants of producer gas. Pellets of N-rich particle board were gasified in an air-blow bubbling bed reactor at 800°C coupled with a downstream HGF unit under different HGF operational conditions. Metallic cartridges with multilayer structure were used as filtration media. The fate of pollutants (tars, NH_3 and HCN) was assessed by complementary analytical techniques and the filter surface was characterised by SEM-EDX. The following conclusions could be drawn:

1) Under reference gasification conditions, tar concentration was 6.5 g/Nm^3 (dry gas, C_6H_6-free) and the nitrogen repartition indicated that approximatively 43% of FBN was converted to NH_3 and 4% to HCN. The rest of FBN was mostly converted to gaseous N_2 and NO_x but, neither one was quantified.

2) The increase in the ER of the reactor showed a marginal impact on tar yield. Lack of major changes on tar composition was ascribed to roughly unchanged reactor bed and freeboard

temperatures with respect to reference tests. Conversely, the yields of NH_3 and HCN rose of 33% and 36%, respectively.

3) A thermal test, conducted by injecting secondary air into the HGF unit without filtration cartridges inside, confirmed that secondary partial oxidation reactions in homogeneous phase took place to a small extent inside the HGF unit. The overall tar yield was unchanged whereas the yields of NH_3 and HCN dropped by 38% and 43%, respectively. Oxidation of NH_3 and HCN was likely catalysed by presence of permanent gases and extended residence time.

4) Oxidative HGF implies secondary reactions in homogeneous and heterogeneous phase. Comparison between thermal and oxidative HGF tests (both conducted with an ER_{HGF}=0.05), provided a way of isolating the effects of heterogeneous reactions. Heterogeneous reactions had a slight impact on gasification indicators and led to a 10% drop in overall tar yield. Oxidation of dust cake particles increased the release of NH_3 as much as 129%.

5) The increase in the secondary air flow rate (until ER_{HGF}=0.1) in the HGF unit resulted in a more severe oxidation of the dust cake particles, rising notably the temperature inside the filter unit and, impacted significantly the gasification indicators. SEM images evidenced the occurrence of irreversible melting, aggregation and sintering phenomena of ash deposits formed in the porosity of the filter. Overall tar yield dropped substantially with the increase in the secondary air flow rate and, a simultaneous release-oxidation mechanism was proposed to explain variations observed in NH_3 and HCN yields.

6) Dust loading on the filter surface showed a minor effect on gasification indicators and tar content, suggesting that heterogeneous reactions inside the HGF unit mainly arose from the

751 interaction between the molecules transported in the gas phase and the dense non-woven
752 metal fibre layer of the filter.

753 Finally, this study showed that for oxidative HGF at mild temperature (400-600°C), secondary air flow
754 rate should be carefully controlled and limited to $ER_{HGF} \leq 0.05$, in order to minimise the exothermic
755 oxidation of dust cake particles, which lead to the formation of ash deposits that impact negatively
756 long-term operation. Further studies should assess the long-term behaviour of metallic cartridges
757 under oxidative conditions and mild-hot temperature, and compare it with the behaviour of standard
758 ceramic candles.

759

760 ## Acknowledgements

761 The authors thank the ADEME, France (Adelither - project N°1702C0042), for the financial support.
762 The authors also thank Matthieu Campargue from RAGT energies and Lucia Jimenez and Mazen Al-
763 Haddad from Leroux et Lotz technologies for their support on material characterization and technical
764 discussions.

765

766

767

768

769

770

5. References

[1] L. Devi, K.J. Ptasinski, F.J.J.G. Janssen, A review of the primary measures for tar elimination in biomass gasification processes, Biomass and Bioenergy. 24 (2003) 125–140. https://doi.org/10.1016/S0961-9534(02)00102-2.

[2] P.J. Woolcock, R.C. Brown, A review of cleaning technologies for biomass-derived syngas, Biomass and Bioenergy. 52 (2013) 54–84. https://doi.org/10.1016/j.biombioe.2013.02.036.

[3] M.L. Valderrama Rios, A.M. González, E.E.S. Lora, O.A. Almazán del Olmo, Reduction of tar generated during biomass gasification: A review, Biomass and Bioenergy. 108 (2018) 345–370. https://doi.org/10.1016/j.biombioe.2017.12.002.

[4] S. Heidenreich, Hot gas filtration – A review, Fuel. 104 (2013) 83–94. https://doi.org/10.1016/j.fuel.2012.07.059.

[5] H. Egsgaard, J. Ahrenfeldt, P. Ambus, K. Schaumburg, U.B. Henriksen, Gas cleaning with hot char beds studied by stable isotopes, Journal of Analytical and Applied Pyrolysis. 107 (2014) 174–182. https://doi.org/10.1016/j.jaap.2014.02.019.

[6] G. Ravenni, Z. Sárossy, J. Ahrenfeldt, U.B. Henriksen, Activity of chars and activated carbons for removal and decomposition of tar model compounds – A review, Renewable and Sustainable Energy Reviews. 94 (2018) 1044–1056. https://doi.org/10.1016/j.rser.2018.07.001.

[7] D.A. Buentello-Montoya, X. Zhang, J. Li, The use of gasification solid products as catalysts for tar reforming, Renewable and Sustainable Energy Reviews. 107 (2019) 399–412. https://doi.org/10.1016/j.rser.2019.03.021.

[8] S. Tuomi, E. Kurkela, P. Simell, M. Reinikainen, Behaviour of tars on the filter in high temperature filtration of biomass-based gasification gas, Fuel. 139 (2015) 220–231. https://doi.org/10.1016/j.fuel.2014.08.051.

[9] L. Dong, M. Asadullah, S. Zhang, X.-S. Wang, H. Wu, C.-Z. Li, An advanced biomass gasification technology with integrated catalytic hot gas cleaning: Part I. Technology and initial

796 experimental results in a lab-scale facility, Fuel. 108 (2013) 409–416.
797 https://doi.org/10.1016/j.fuel.2012.11.043.
798 [10] S. Zhang, M. Asadullah, L. Dong, H.-L. Tay, C.-Z. Li, An advanced biomass gasification technology
799 with integrated catalytic hot gas cleaning. Part II: Tar reforming using char as a catalyst or as a
800 catalyst support, Fuel. 112 (2013) 646–653. https://doi.org/10.1016/j.fuel.2013.03.015.
801 [11] S. Zhang, Y. Song, Y.C. Song, Q. Yi, L. Dong, T.T. Li, L. Zhang, J. Feng, W.Y. Li, C.-Z. Li, An advanced
802 biomass gasification technology with integrated catalytic hot gas cleaning. Part III: Effects of
803 inorganic species in char on the reforming of tars from wood and agricultural wastes, Fuel. 183
804 (2016) 177–184. https://doi.org/10.1016/j.fuel.2016.06.078.
805 [12] S. Heidenreich, P.U. Foscolo, New concepts in biomass gasification, Progress in Energy and
806 Combustion Science. 46 (2015) 72–95. https://doi.org/10.1016/j.pecs.2014.06.002.
807 [13] M. Nacken, G.V. Baron, S. Heidenreich, S. Rapagnà, A. D'Orazio, K. Gallucci, J.F.M. Denayer, P.U.
808 Foscolo, New DeTar catalytic filter with integrated catalytic ceramic foam: Catalytic activity
809 under model and real bio syngas conditions, Fuel Processing Technology. 134 (2015) 98–106.
810 https://doi.org/10.1016/j.fuproc.2015.01.020.
811 [14] F. García-Labiano, P. Gayán, L.F. de Diego, A. Abad, T. Mendiara, J. Adánez, M. Nacken, S.
812 Heidenreich, Tar abatement in a fixed bed catalytic filter candle during biomass gasification in a
813 dual fluidized bed, Applied Catalysis B: Environmental. 188 (2016) 198–206.
814 https://doi.org/10.1016/j.apcatb.2016.02.005.
815 [15] L.F. de Diego, F. García-Labiano, P. Gayán, A. Abad, T. Mendiara, J. Adánez, M. Nacken, S.
816 Heidenreich, Tar abatement for clean syngas production during biomass gasification in a dual
817 fluidized bed, Fuel Processing Technology. 152 (2016) 116–123.
818 https://doi.org/10.1016/j.fuproc.2016.05.042.
819 [16] A. D'Orazio, S. Rapagnà, P.U. Foscolo, K. Gallucci, M. Nacken, S. Heidenreich, A. Di Carlo, A.
820 Dell'Era, Gas conditioning in H2 rich syngas production by biomass steam gasification:
821 Experimental comparison between three innovative ceramic filter candles, International

822 Journal of Hydrogen Energy. 40 (2015) 7282–7290.
823 https://doi.org/10.1016/j.ijhydene.2015.03.169.
824 [17] E. Simeone, M. Siedlecki, M. Nacken, S. Heidenreich, W. de Jong, High temperature gas
825 filtration with ceramic candles and ashes characterisation during steam–oxygen blown
826 gasification of biomass, Fuel. 108 (2013) 99–111. https://doi.org/10.1016/j.fuel.2011.10.030.
827 [18] E. Kurkela, M. Kurkela, I. Hiltunen, Steam–oxygen gasification of forest residues and bark
828 followed by hot gas filtration and catalytic reforming of tars: Results of an extended time test,
829 Fuel Processing Technology. 141 (2016) 148–158.
830 https://doi.org/10.1016/j.fuproc.2015.06.005.
831 [19] L. Lang, W. Yang, J. Xie, X. Yin, C. Wu, J.Y.S. Lin, Oxidative filtration for flyash & tar removal from
832 1.0 MWth fixed-bed biomass air gasification, Biomass and Bioenergy. 122 (2019) 145–155.
833 https://doi.org/10.1016/j.biombioe.2019.01.018.
834 [20] D. Fuentes-Cano, L. von Berg, A. Diéguez-Alonso, R. Scharler, A. Gómez-Barea, A. Anca-Couce,
835 Tar conversion of biomass syngas in a downstream char bed, Fuel Processing Technology. 199
836 (2020) 106271. https://doi.org/10.1016/j.fuproc.2019.106271.
837 [21] GKD DE | World Wide Weave, (n.d.). https://www.gkd-group.com/de-de/ (accessed February 6,
838 2021).
839 [22] H. Zhan, X. Zhuang, Y. Song, J. Liu, S. Li, G. Chang, X. Yin, C. Wu, X. Wang, A review on evolution
840 of nitrogen-containing species during selective pyrolysis of waste wood-based panels, Fuel. 253
841 (2019) 1214–1228. https://doi.org/10.1016/j.fuel.2019.05.122.
842 [23] P. Girods, Y. Rogaume, A. Dufour, C. Rogaume, A. Zoulalian, Low-temperature pyrolysis of wood
843 waste containing urea-formaldehyde resin, Renewable Energy. 33 (2008) 648–654.
844 https://doi.org/10.1016/j.renene.2007.03.026.
845 [24] B.C. Williams, D. Mcilveen-Wright, S. Rezvani, Gasification of Waste Medium Density
846 Fibreboard as a Route to Power Generation, Developments in Chemical Engineering and
847 Mineral Processing. 11 (2003) 55–66. https://doi.org/10.1002/apj.5500110206.

[25] M. Hervy, D. Remy, A. Dufour, G. Mauviel, Air-blown gasification of Solid Recovered Fuels (SRFs) in lab-scale bubbling fluidized-bed: Influence of the operating conditions and of the SRF composition, Energy Conversion and Management. 181 (2019) 584–592. https://doi.org/10.1016/j.enconman.2018.12.052.

[26] M. Neubert, S. Reil, M. Wolff, D. Pöcher, H. Stork, C. Ultsch, M. Meiler, J. Messer, L. Kinzler, M. Dillig, S. Beer, J. Karl, Experimental comparison of solid phase adsorption (SPA), activated carbon test tubes and tar protocol (DIN CEN/TS 15439) for tar analysis of biomass derived syngas, Biomass and Bioenergy. 105 (2017) 443–452. https://doi.org/10.1016/j.biombioe.2017.08.006.

[27] R. Olcese, V. Carré, F. Aubriet, A. Dufour, Selectivity of bio-oils catalytic hydrotreatment assessed by petroleomic and GC*GC/MS-FID analysis, Energy and Fuels. 27 (2013) 2135–2145. https://doi.org/10.1021/ef302145g.

[28] J.-Y. de Saint Laumer, E. Cicchetti, P. Merle, J. Egger, A. Chaintreau, Quantification in Gas Chromatography: Prediction of Flame Ionization Detector Response Factors from Combustion Enthalpies and Molecular Structures, Anal. Chem. 82 (2010) 6457–6462. https://doi.org/10.1021/ac1006574.

[29] J. Kister, N. Pieri, R. Alvarez, M.A. Díez, J.J. Pis, Effects of Preheating and Oxidation on Two Bituminous Coals Assessed by Synchronous UV Fluorescence and FTIR Spectroscopy, Energy Fuels. 10 (1996) 948–957. https://doi.org/10.1021/ef950159a.

[30] T. Vo-Dinh, P.R. Martinez, Direct determination of selected polynuclear aromatic hydrocarbons in a coal liquefaction product by synchronous luminescence techniques, Analytica Chimica Acta. 125 (1981) 13–19.

[31] J.R. Kershaw, C. Sathe, J. Hayashi, C.-Z. Li, T. Chiba, Fluorescence Spectroscopic Analysis of Tars from the Pyrolysis of a Victorian Brown Coal in a Wire-Mesh Reactor, Energy Fuels. 14 (2000) 476–482. https://doi.org/10.1021/ef990181u.

873 [32] C. Berrueco, J. Recari, S. Abelló, X. Farriol, D. Montané, Experimental Investigation of Solid
874 Recovered Fuel (SRF) Gasification: Effect of Temperature and Equivalence Ratio on Process
875 Performance and Release of Minor Contaminants, Energy Fuels. 29 (2015) 7419–7427.
876 https://doi.org/10.1021/acs.energyfuels.5b02032.
877 [33] K.M. Broer, P.A. Johnston, A. Haag, R.C. Brown, Resolving inconsistencies in measurements of
878 hydrogen cyanide in syngas, Fuel. 140 (2015) 97–101.
879 https://doi.org/10.1016/j.fuel.2014.09.069.
880 [34] L.P.L.M. Rabou, R.W.R. Zwart, B.J. Vreugdenhil, L. Bos, Tar in Biomass Producer Gas, the Energy
881 research Centre of The Netherlands (ECN) Experience: An Enduring Challenge, Energy Fuels. 23
882 (2009) 6189–6198. https://doi.org/10.1021/ef9007032.
883 [35] S. Nilsson, A. Gómez-Barea, I. Pardo-Arias, M. Suárez-Almeida, V.F. de Almeida, Comparison of
884 Six Different Biomass Residues in a Pilot-Scale Fluidized Bed Gasifier, Energy Fuels. (2019).
885 https://doi.org/10.1021/acs.energyfuels.9b01513.
886 [36] D.T. Pio, L.A.C. Tarelho, M.A.A. Matos, Characteristics of the gas produced during biomass
887 direct gasification in an autothermal pilot-scale bubbling fluidized bed reactor, Energy. 120
888 (2017) 915–928. https://doi.org/10.1016/j.energy.2016.11.145.
889 [37] S.V.B. Van Paasen, J.H.A. Kiel, Tar formation in a fluidised-bed gasifier: Impact of fuel properties
890 and operating conditions, Energy research Centre of the Netherlands ECN, 2004.
891 [38] T. Katoh, S. Yokoyama, Y. Sanada, Analysis of a coal-derived liquid using highpressure liquid
892 chromatography and synchronous fluorescence spectrometry, Fuel. 59 (1980) 845–850.
893 https://doi.org/10.1016/0016-2361(80)90033-2.
894 [39] H. Sharma, V.K. Jain, Z.H. Khan, Use of constant wavelength synchronous spectrofluorimetry for
895 identification of polycyclic aromatic hydrocarbons in air particulate samples, Spectrochimica
896 Acta Part A: Molecular and Biomolecular Spectroscopy. 108 (2013) 268–273.
897 https://doi.org/10.1016/j.saa.2013.01.079.

[40] Z. Wang, C. Wei, H. Shui, S. Ren, C. Pan, Z. Wang, H. Li, Z. Lei, Synchronous fluorimetric characterization of heavy intermediates of coal direct liquefaction, Fuel. 98 (2012) 67–72.

[41] J.B.F. Lloyd, I.W. Evett, Prediction of peak wavelengths and intensities in synchronously excited fluorescence emission spectra, Anal. Chem. 49 (1977) 1710–1715. https://doi.org/10.1021/ac50020a020.

[42] T. Vo-Dinh, Multicomponent analysis by synchronous luminescence spectrometry, Anal. Chem. 50 (1978) 396–401. https://doi.org/10.1021/ac50025a010.

[43] Z. Benkhedda, P. Landais, J. Kister, J.M. Dereppe, M. Monthioux, Spectroscopic analyses of aromatic hydrocarbons extracted from naturally and artificially matured coals, Energy Fuels. 6 (1992) 166–172. https://doi.org/10.1021/ef00032a008.

[44] V. Wilk, H. Hofbauer, Conversion of fuel nitrogen in a dual fluidized bed steam gasifier, Fuel. 106 (2013) 793–801. https://doi.org/10.1016/j.fuel.2012.12.056.

[45] S.Q. Turn, C.M. Kinoshita, D.M. Ishimura, J. Zhou, The fate of inorganic constituents of biomass in fluidized bed gasification, Fuel. 77 (1998) 135–146. https://doi.org/10.1016/S0016-2361(97)00190-7.

[46] P. Glarborg, J.A. Miller, B. Ruscic, S.J. Klippenstein, Modeling nitrogen chemistry in combustion, Progress in Energy and Combustion Science. 67 (2018) 31–68. https://doi.org/10.1016/j.pecs.2018.01.002.

[47] C. Mandl, I. Obernberger, I.R. Scharler, Characterisation of fuel bound nitrogen in the gasification process and the staged combustion of producer gas from the updraft gasification of softwood pellets, Biomass and Bioenergy. 35 (2011) 4595–4604. https://doi.org/10.1016/j.biombioe.2011.09.001.

[48] I. Narváez, A. Orío, M.P. Aznar, J. Corella, Biomass Gasification with Air in an Atmospheric Bubbling Fluidized Bed. Effect of Six Operational Variables on the Quality of the Produced Raw Gas, Ind. Eng. Chem. Res. 35 (1996) 2110–2120. https://doi.org/10.1021/ie9507540.

[49] M. Campoy, A. Gómez-Barea, D. Fuentes-Cano, P. Ollero, Tar Reduction by Primary Measures in an Autothermal Air-Blown Fluidized Bed Biomass Gasifier, Ind. Eng. Chem. Res. 49 (2010) 11294–11301. https://doi.org/10.1021/ie101267c.

[50] K.M. Broer, R.C. Brown, Effect of Equivalence Ratio on Partitioning of Nitrogen during Biomass Gasification, Energy Fuels. 30 (2016) 407–413. https://doi.org/10.1021/acs.energyfuels.5b02197.

[51] J. Jiang, L. Lang, L. Lin, H. Liu, X. Yin, C. Wu, Partial Oxidation of Filter Cake Particles from Biomass Gasification Process in the Simulated Product Gas Environment, Energy Fuels. 32 (2018) 1703–1710. https://doi.org/10.1021/acs.energyfuels.7b01100.

[52] A. Gómez-Barea, P. Ollero, B. Leckner, Optimization of char and tar conversion in fluidized bed biomass gasifiers, Fuel. 103 (2013) 42–52. https://doi.org/10.1016/j.fuel.2011.04.042.

[53] N. Peng, C. Huang, J. Su, An experimental and kinetic study of thermal decomposition of phenanthrene, Journal of Hazardous Materials. 365 (2019) 565–571. https://doi.org/10.1016/j.jhazmat.2018.11.026.

[54] C. Gai, Y. Dong, S. Yang, Z. Zhang, J. Liang, J. Li, Thermal decomposition kinetics of light polycyclic aromatic hydrocarbons as surrogate biomass tar, RSC Adv. 6 (2016) 83154–83162. https://doi.org/10.1039/C6RA15513H.

[55] Ø. Skreiberg, P. Kilpinen, P. Glarborg, Ammonia chemistry below 1400 K under fuel-rich conditions in a flow reactor, Combustion and Flame. 136 (2004) 501–518. https://doi.org/10.1016/j.combustflame.2003.12.008.

[56] V.J. Wargadalam, G. Löffler, F. Winter, H. Hofbauer, Homogeneous formation of NO and N2O from the oxidation of HCN and NH3 at 600–1000°C, Combustion and Flame. 120 (2000) 465–478. https://doi.org/10.1016/S0010-2180(99)00107-8.

[57] U. Kleinhans, C. Wieland, F.J. Frandsen, H. Spliethoff, Ash formation and deposition in coal and biomass fired combustion systems: Progress and challenges in the field of ash particle sticking

948 and rebound behavior, Progress in Energy and Combustion Science. 68 (2018) 65–168.
949 https://doi.org/10.1016/j.pecs.2018.02.001.
950 [58] M. Zevenhoven-Onderwater, R. Backman, B.-J. Skrifvars, M. Hupa, The ash chemistry in
951 fluidised bed gasification of biomass fuels. Part I: predicting the chemistry of melting ashes and
952 ash–bed material interaction, Fuel. 80 (2001) 1489–1502. https://doi.org/10.1016/S0016-
953 2361(01)00026-6.
954 [59] X. Yao, Y. Hu, J. Ge, X. Ma, J. Mao, L. Sun, K. Xu, K. Xu, A comprehensive study on influence of
955 operating parameters on agglomeration of ashes during biomass gasification in a laboratory-
956 scale gasification system, Fuel. 276 (2020) 118083. https://doi.org/10.1016/j.fuel.2020.118083.
957 [60] X. Yao, H. Zhou, Z. Zhao, K. Xu, Research on dependence of concentration and transformation
958 of inorganics in biomass gasification ashes upon particle size classification, Powder Technology.
959 371 (2020) 1–12. https://doi.org/10.1016/j.powtec.2020.05.083.
960 [61] R.T.K. Baker, The relationship between particle motion on a graphite surface and Tammann
961 temperature, Journal of Catalysis. 78 (1982) 473–476.
962 [62] G. Lardier, J. Kaknics, A. Dufour, R. Michel, B. Cluet, O. Authier, J. Poirier, G. Mauviel, Gas and
963 Bed Axial Composition in a Bubbling Fluidized Bed Gasifier: Results with Miscanthus and
964 Olivine, Energy Fuels. 30 (2016) 8316–8326. https://doi.org/10.1021/acs.energyfuels.6b01816.
965 [63] X. Yao, Z. Zhao, K. Xu, H. Zhou, Determination of ash forming characteristics and
966 fouling/slagging behaviours during gasification of masson pine in a fixed-bed gasifier,
967 Renewable Energy. 160 (2020) 1420–1430. https://doi.org/10.1016/j.renene.2020.06.008.
968 [64] G. Ravenni, Z. Sárossy, S. Sanna, J. Ahrenfeldt, U.B. Henriksen, Residual gasification char applied
969 to tar reforming in a pilot-scale gasifier: Performance and evolution of char properties for
970 perspective cascade uses, Fuel Processing Technology. 210 (2020) 106546.
971 https://doi.org/10.1016/j.fuproc.2020.106546.
972 [65] G. Ravenni, O.H. Elhami, J. Ahrenfeldt, U.B. Henriksen, Y. Neubauer, Adsorption and
973 decomposition of tar model compounds over the surface of gasification char and active carbon

within the temperature range 250–800 °C, Applied Energy. 241 (2019) 139–151. https://doi.org/10.1016/j.apenergy.2019.03.032.

[66] X. Jing, Z. Wang, Z. Yu, Q. Zhang, C. Li, Y. Fang, Experimental and Kinetic Investigations of CO2 Gasification of Fine Chars Separated from a Pilot-Scale Fluidized-Bed Gasifier, Energy Fuels. 27 (2013) 2422–2430. https://doi.org/10.1021/ef4002296.

[67] M. Ruiz, E. Martin, J. Blin, L. Van de Steene, F. Broust, Understanding the Secondary Reactions of Flash Pyrolysis Vapors inside a Hot Gas Filtration Unit, Energy Fuels. 31 (2017) 13785–13795. https://doi.org/10.1021/acs.energyfuels.7b02923.

[68] H.-P. Schmidt, European Biochar Certificate (EBC) - guidelines version 6.1, 2015. https://doi.org/10.13140/RG.2.1.4658.7043.

Graphical abstract